Discordant perturbations of transcriptome and epigenome landscapes highlight dual roles of proinflammatory players in normal and IL1B-compromised OPC maturation trajectory in a prenatal model of diffuse white matter injury

Anne-Laure SCHANG[1,2,3,4,&], Juliette van STEENWINCKEL[3,4,§], Julia LIPECKI[6,§], Charlotte RICH[5,6], Kate WOLLEY-ALLEN[5], Nigel DYER[5], Tifenn Le CHARPENTIER[3,4], Bobbi FLEISS[3,4,7], Patrick SCHÄFER[5], Sascha OTT[6,$,*], Valérie MEZGER[1,2,3,*], Délara SABÉRAN-DJONEIDI[1,2,3,$,*], Pierre GRESSENS[3,4,7,*]

[1] CNRS, UMR7216 Épigénétique et Destin Cellulaire, F-75205 Paris Cedex 13, France
[2] Univ Paris Diderot, Sorbonne Paris Cité, F-75205 Paris Cedex 13, France
[3] Département Hospitalo-Universitaire DHU PROTECT, Paris, France

[4] PROTECT, INSERM, Université Paris Diderot, Sorbonne Paris Cité, F-75019 Paris, France
[5] University of Warwick, Coventry, CV4 7AL, United Kingdom
[6] Warwick Systems Biology Centre, University of Warwick, Coventry, CV4 7AL, United Kingdom
[7] Centre for the Developing Brain, Department of Division of Imaging Sciences and Biomedical Engineering, King's College London, King's Health Partners, St. Thomas' Hospital, London, SE1 7EH, United Kingdom.

[§] Equal contribution to the work
[*] equal contribution to the direction of the work

[$]co-corresponding authors

[&] Present address: UMR CNRS 8638-Chimie Toxicologie Analytique et Cellulaire, Université Paris Descartes, Sorbonne Paris Cité, Faculté de Pharmacie de Paris, 4 Avenue de l'Observatoire, 75006 Paris, France

FUNDING Information
VM was funded by Agence Nationale de la Recherche (« HSF-EPISAME », SAMENTA ANR-13-SAMA-0008-01) and FRA 2015/16. DSD was funded by Paris Diderot University for travel grant for SO. ALS was supported by a postdoctoral fellowship by SAMENTA ANR-13-SAMA-0008-01. The supporting bodies played no role in any aspect of study design, analysis, interpretation or decision to publish this data.
PG was funded by Inserm, Paris Diderot University, Fondation Grace de Monaco, PremUP, Fondation des Gueules Cassées, and an additional grant from "Investissement d'Avenir -ANR-11-INBS-0011-" NeurATRIS. PG and BF acknowledge financial support from the Department of Health via the National Institute for Health Research (NIHR) comprehensive Biomedical Research Centre award to Guy's & St Thomas' NHS Foundation Trust in partnership with King's College London and King's College Hospital NHS Foundation Trust. The supporting bodies played no role in any aspect of study design, analysis, interpretation or decision to publish this data.

Abstract

Premature birth is the commonest cause of death and disability in children under 5 years of age. Diffuse white matter injury (DWMI) is one of the hallmarks of neurological damages associated to premature birth, and is associated with increased risk of autism spectrum disorders. DWMI is due to maturation arrest in oligodendrocyte precursors (OPCs), consequently leads to cortical hypomyelination, and is provoked by inflammatory insults accompanying premature birth. The lack of therapeutic solutions is a strong hint to unveil the molecular mechanisms underlying the persistent impact of neuroinflammation on OPC cell fate. We took advantage of a validated mouse model of DWMI, based on interleukin 1B (IL1B) intraperitoneal administration from postnatal days 1 to 5 (P1-P5), which recapitulates OPCs maturational arrest. Using integrated genome-wide approaches, we challenged the robustness versus vulnerability of epigenome and transcriptome at the end of IL1B exposure, in a purified population of premyelinating OPCs. We evidenced limited epigenomic disturbances in ILB1-treated OPCs, but, in contrast, marked transcriptomic alterations, linked to abnormally sustained activation of immune/inflammatory and corresponding transcription factor pathways. These genes are indeed expressed in unstressed OPCs and we show that they are physiologically downregulated along the normal P0-P5 developmental OPC trajectory. Rather than provoking major changes in genome-wide chromatin accessibility, neuroinflammation takes advantage of open chromatin regions and active transcriptional programs at the time of exposure, and deeply counteracts their stage-dependent regulation by sustained upregulation of their transcript levels. The same transcription factors are not only involved in the stress-responsive upregulation of target genes of the immune/inflammatory pathways in OPC exposed to IL1B, but also in the expression of the same inflammatory players in unstressed OPCs, during their normal stage-dependent maturation. The encounter of their potential developmental role in OPC trajectory and their stress-responsive action upon ILB1 exposure paves the way for intricate interference between the response to neuroinflammatory insults and the white matter developmental program, likely contributing to OPC maturation arrest.

INTRODUCTION

Premature birth (13 % of all births in the USA) is the commonest cause of death and disability in children under 5 years of age. These disastrous effects are predominantly due to neurological damage, which majorly includes an array of lesions, collectively called "encephalopathy of prematurity". Almost 10% of infants born before 33 weeks (a normal pregnancy lasts 40-42 weeks) develop cerebral palsy and approximately 35% have persistent cognitive and neuropsychiatric deficits, including autism spectrum disorders and attention deficit/hyperactivity disorder. Although the most severe problems stem from extreme prematurity, even slight reductions in gestational length have significant adverse effects. One of the hallmarks of encephalopathy of prematurity is diffuse white matter injury (DWMI). DWMI is considered a key target for neuroprotection and the prevention of long-lasting handicap, and is due to oligodendrocyte maturation arrest, leading to hypomyelination and ultimately to defects in grey matter connectivity (1-3). In that context, neuroinflammation is a leading cause of encephalopathy of prematurity, serving as a central mediator of oligodendrocyte maturational deficits and hypomyelination (4-6).

We have previously validated a mouse model of encephalopathy of prematurity, using interleukin 1B (IL1B) intraperitoneal administration from postnatal days 1 to 5 (P1-P5), which recapitulates maturational arrest in oligodendrocytes (7,8). Despite the fact that exposure to inflammation is limited in time (5 days in our mouse model), the OPC maturation blockade persists, leading to long-term myelination defects (7). This suggests that these prenatal adversities cause deviations from the delicately choreographed programs that control OPC maturation, creating a cell fate conflict.

Here, using a purified population of premyelinating OPCs and integrated genome-wide approaches, we have explored the contribution of epigenomic and transcriptomic disturbances in the OPC cell fate issue. **1)** We show that at P5 a limited number of chromatin regions are perturbed. **2)** On the top of the genes whose expression is significantly altered by IL1B, we found genes involved in the immune system and inflammatory response. These genes, including cytokines and chemokines, are unexpectedly expressed by OPC themselves, in normal conditions, in a physiological, and developmental manner in OPCs at early stages, and downregulated at further steps of their maturation. The stage-dependent downregulation of these genes is counteracted by IL1B, which provokes a strong upregulation of their expression – likely participating to a cell fate issue.

These major transcriptomic disturbances surprisingly occur in genes, which exhibit no overt changes in chromatin accessibility at P5: indeed, neuroinflammation takes advantage of transcriptional programs, which are already active at the time of exposure - namely chromatin regions, which are already open - and disturbs their developmental regulation.

We have therefore unraveled a mechanism by which neuroinflammation acts on OPCs in a model mimicking prenatal chronic inflammation in human. Indeed, the unexpected expression of inflammatory players by unstressed OPCs during their normal and stage-dependent maturation likely paves the way for intricate interference between the response to neuroinflammatory insults and the white matter developmental program.

RESULTS

The epigenome of OPCs is globally preserved in response to systemic IL1B exposure

We first investigated the impact of IL1B on the integrity of the chromatin landscape in OPCs, using ATAC-Seq (9; *Assay for Transposase-Accessible Chromatin with high-throughput sequencing*; Fig. 1). This epigenomic approach is based on the properties of the Tn5 transposase to integrate a transposon in the open chromatin regions, and allowing, by this insertion, an exquisite mapping of the boundaries of these accessible regions. IL1B was administrated by intraperitoneal injections to pups (versus PBS, as a control; Fig. 1; 7,8) between P1 and P5. This time schedule mimics chronic exposure to circulating inflammatory players (cytokines) during the third trimester of human pregnancy. Indeed, P5 shows similarities with human gestational age around 32 weeks. Using

magnetic-activated cell sorting (MACS), we isolated at P5 the major maturating, premyelinating OPC population, positive for the O4 expression marker (O4+ OPCs). This marker is present in the human preterm and mouse neonate cortex, and affected by IL1B injections (7, 10; Fig. 1). RT-qPCR analyses demonstrated that the O4+ cell population expressed high levels of *Myelin binding protein* (*Mbp*) mRNAs, but very low levels of the microglia marker mRNAs, CD11B (*Itgam*, *Integrin alpha M* gene) compared with microglial (CD11+) cells (Fig. S1*A*). Note that we collected comparable numbers of O4+ OPCs from control (PBS) and treated (IL1B) samples (1.12×10^6+/- 0.12×10^6). Using the bioinformatics workflow described in Fig. S1*B*, including MACS2 and EdgeR software, we obtained an average of 72 million Tn5-integrated mapped reads per PBS or IL1B-treated sample, representing a total of 213,246 statistically significant peaks (MACS2; FDR < 0.05; Table S1 and S2; Dataset S1). Analysis of insert size distribution revealed resolved nucleosome profiles (Fig. S1*C*).

We performed principle component analysis (PCA) on our samples and observed that, on the one hand, principal component 1 (PC1; corresponding to 42% variance) separated PBS-treated (PBS1 to 3) from IL1B-treated (IL1B1 to 3) samples (Fig. 2*A*). This suggests that the majority of the variance in this dataset can be explained by the IL1B treatment. Using EdgeR MDS function, we obtained similar results (Fig. S2*A*). Among the 213,245 significant peaks, only 524 peaks were differentially open or closed in response to IL1B (FDR < 0.05, Fig. 2*B*; Fig. S2*B*; Table S3). The majority of peaks with differential chromatin accessibility was more open in IL1B, compared to PBS conditions (Fig. 2*B,* Fig. 2*C*). Peaks were mostly distributed in intergenic and intronic regions and were enriched in gene regulatory regions and gene bodies (Fig. S2*C*). A similar distribution was observed for the total number of differentially open or closed peaks (data not shown). Representative peaks showing increased, reduced, or unchanged chromatin accessibility are illustrated in Fig. 2*D* and Fig. S2*D*. Gene ontology analyses using David6.8 showed that the genes whose TSS is located the closest to the 524 peaks, and thus likely associated with major chromatin alteration, exhibited a tendency - but not statistically significant (FDR > 0.05)- to belong to pathways (GO-terms) relevant for neural development (regulation of cell migration, cell adhesion, neuron projection development etc.; Fig. S2*E*; Table S4).

Our results thus reveal that around 0.25% of regions shows differentially opening or closing of the chromatin landscape at P5.

Impact of systemic IL1B exposure on the transcriptome of O4+ OPCs

We analyzed gene expression in isolated O4+ OPCs from male cortices in each condition (Fig. 1*A*) using microarrays. We compared six independent samples, corresponding to IL1B exposure, to six independent samples, corresponding to PBS (control) conditions. IL1B exposure mainly provoked upregulation of gene expression: 1,266 genes were up-regulated and 454 downregulated, which corresponded to 1,872 and 699 probes, respectively (FC +/-1.5; FDR < 0.05; Fig. 3*A*; Dataset S2; Table S5). The analysis of our microarray data revealed that the expression of genes involved in myelination (which are still lowly expressed at P5 in normal conditions) was downregulated by IL1B at this stage, whereas that of *Id2*, a progenitor cell marker that inhibits OPC differentiation, was upregulated, as expected (7; (Fig. 3*B*). We confirmed these results by RT-qPCR performed on additional O4+ OPC RNA samples, from independent experiments (Fig. 3*C*). Altogether, these results indicated that our samples and microarray analyses were representative of OPC maturation blockade (7; Fig. 3*B*). The GO analysis of these upregulated genes strikingly pinpointed the immune system and inflammatory response in the top 5 most statistically significant pathways (DAVID 6.8; Fig. 3*D*; Table S6). The analysis of downregulated genes indicated that they belonged to pathways linked to development (Fig. S3). The expression profiles of the 262 genes belonging to the immune system and inflammatory response pathways in our microarray data highlighted massive upregulation, compared to downregulation (Fig. 3*E*). Using RT-qPCR on independent samples, we confirmed the induction of the expression of known players of these pathways: cytokines, chemokines, interleukines and their receptors (Fig. 3*F*).

OPCs intrinsically activate genes of the immune and inflammatory pathways in response to IL1B

To exclude the possibility that the upregulation of players of the immune system and inflammatory response was due to contamination of O4+ OPCs with microglia, we performed a series of experiments. We have previously shown that the same paradigm of neuroinflammation by IL1B activated microglia, and published microarray analyses of transcriptomic profiles in microglia (CD11+ MACS-isolated cells: +/-IL1B; 8). These data have been obtained from the same series of animals as the O4+ OPC populations examined in this paper by microarrays (Fig. 1), by sequentially MACS-isolated O4+ OPCs and CD11+ microglia cells from the same brains. We thus compared the microarray gene expression profiles in CD11+ cells to the list of 262 genes found in OPCs corresponding to these pathways (Fig. 4*A*; Fig. S4; dataset from 8). We showed that these two cell populations exhibited remarkable differences in gene expression profiles at P5, in response to IL1B, both in terms of magnitude and direction (down- versus upregulation; Fig. 4*A*; Fig. S4). These data were confirmed by RT-qPCR in independent O4+ OPC and CD11+ samples, and extended to astrocytes (GLAST+). Neither microglia cells, nor astrocytes showed increase in the expression of cytokines and chemokines at P5 (illustrated here for *Ccl2*, *Cxcl1* and *Cxcl10*; Fig. 4*B*).

Altogether, these results indicate that the upregulation of immune and inflammatory pathway in O4+ OPCs in response to IL1B in our microarray analyses at P5 cannot be attributed to contamination of OPCs by microglia cells. Notably, the upregulation of these genes in microglia was maximal at P1 and their expression at P5 has already recovered, reaching basal levels comparable to that of PBS samples (8; Fig. 4*B*; ratio 1:1).

To further challenge the IL1B-induced production of inflammatory players by OPCs, we then isolated primary OPCs, grew them *in vitro* and treated these cultures with IL1B (Fig. 5*A*). Using *Luminex,* we detected significant induction of the production of cytokine and chemokine proteins, in the supernatant of IL1B-treated MACS-isolated primary O4+ OPCs, cultured for 24 or 72 hours (Fig. 5*B*). We also confirmed the upregulation of these players at mRNA levels (Fig. S5*A*).
In conclusion, these data strongly support the hypothesis that P5 O4+ OPCs are able to intrinsically synthesize players of the inflammation pathway, in response to IL1B exposure.

Crossing chromatin and transcriptional disturbances in response to IL1B exposure

To examine the contribution of modifications in the chromatin accessibility in these transcriptomic disturbances, we crossed our ATAC-Seq data (213,246 peaks, actually corresponding to 20,108 gene names) and microarray data (limited to annotated genes (with ID); 25,294). We found 16,883 genes in common between the ATAC-Seq and microarray data, of which 1,333 genes had their expression altered by IL1B exposure. Intersecting between the 1,333 genes with the total number of ATAC-Seq peaks showing differential chromatin accessibility (404 peaks) upon IL1B exposure, gave a number of 53 genes whose alterations in expression correlated to opening or closing of the chromatin (Fig. 6*A*; $p= 1.7\ e^{-4}$; Table S7).

We reasoned that peaks corresponding to opening or closing of the chromatin and lying within +/- 8kb around a TSS were most likely susceptible to participate to the regulation of the expression of the corresponding gene. Taking this into account in order to maximize the chance to attribute peaks to relevant genes, we identified 15 genes showing differential expression and exhibiting modifications of the chromatin landscape in their vicinity, which corresponded to 20 % of the ATAC-Seq peaks present in +/- 8 kb round TSS (Fig. 6*B*; $p= 8.74\ e^{-5}$; Table S8). Among these 15 genes, 10 corresponded to genes involved in the immune system and inflammatory response pathways: *Cd14, Cwc22 (*Fig. 2*D), Hmha1, Ifit3, March1, Nckap1l, Slfn2, Slc15a3, Tlr1, Tnfsf14, Tnfrsf12a* (Table S8), (https://www.ncbi.nlm.nih.gov/gene/20556)*, (https://www.genecards.org/cgi-bin/carddisp.pl?gene=SLC15A3*). Interestingly, *Hif3a*, a gene recently identified in models of inflammation, was also identified in the 15-gene list (see discussion; Fig. 2*D*).

In summary, the immune system and inflammatory response pathways were prominently represented in the lists of genes showing marked dysregulation of their expression upon ILB1 treatment, and associated two different chromatin behaviors: 1) a limited number of genes shows

differential chromatin accessibility upon IL1B exposure (Fig. 6*A* and *B*); 2) the bulk of the genes in the top 5 most upregulated genes upon IL1B treatment displays no major changes in chromatin accessibility (Fig. 3*D*). Indeed, in this case, the chromatin was already in an open conformation in the PBS samples (illustrated in Fig. S2*D*).

Identification of TF motifs and binding involved in immune system and inflammatory pathways

Because, in the large majority of the cases, the chromatin was already open, we investigated the putative involvement of transcriptional regulators. We searched for enrichment in TF binding sites (TFBS) using HOMER known motifs in the ATAC-Seq peaks adjacent (+/- 8 kb) to differentially regulated genes (up and downregulated genes ("ALL")). Members of the IRF (interferon-regulatory factor) family appeared at the top of the list with the stronger scoring results, as well as the composite site PU.1-IRF8, and NFκB family members (Fig. S5*B*). A list of similar motifs was found with comparable p-values to the peaks adjacent to upregulated genes ("UP"; Fig. S5*C*)..

We investigated the occurrence of paired motifs in the peaks located in +/- 8Kb regions around the TSS of differentially regulated genes, as described in Materials and Methods. The analysis of peaks corresponding to downregulated genes did not reveal any paired motif enrichment, compared to random occurrence in the whole genome. In contrast, the analyses of ATAC-Seq peaks associated with upregulated genes revealed the existence of paired TFBS motifs, with marked involvement of TFBS from the IRF family, PU.1/SPI1, *Isre* (Interferon-Stimulated Response Element), NFκB, and AP-1 family (Fig. 6*C*; Table S9).

Using the strand-sensitive Wellington algorithm (11), which possesses high accuracy at inferring protein (TF)-DNA interactions, we challenged the actual occupancy of such TFs on DNA in PBS and IL1B conditions. We investigated the presence of footprints corresponding to occupied TFBS and their motif content, located within significant ATAC-Seq peaks, adjacent to differentially regulated genes. The average footprint profiles, produced for the top 6 results in the list of known HOMER motifs are illustrated, for the "ALL" genes for IRF1, IRF2, IRSE and NFκB Fig. 6*D* (Both conditions, PBS plus IL1B) and in Fig. S6*A* (PBS, upper panels; IL1B, lower panels). The dip in the number of peaks at the center of the sharp average profile (indicated by brackets) was strongly suggestive of effective TF binding. A similar analysis is illustrated for IRF1, IRF2, IRSE, and NFκB (Fig. S6*C*). In contrast, PU.1-IRF8 and PGR (Progesterone Receptor) average footprint exhibited sharp internal peak, suggestive of transposon insertion bias (37, Fig. S6*B*). Interestingly, there was little difference in the average footprint profiles for all these TFs, when considering PBS samples only, IL1B samples only, or both conditions together, indicating that these TFs might already bind DNA at the corresponding motifs in PBS conditions.

Altogether, these results indicate that key TFs involved in the immunity and inflammatory processes are bound in a significant number of open regions located in the vicinity of genes that are differentially upregulated by IL1B. The binding of such TFs is coherent with the prominent upregulation of proinflammatory cytokine and chemokine genes, and other genes of the immune system and inflammatory pathways. In addition, because footprint profiles were similar in PBS and IL1B conditions, this suggested that, at P5, these TFs might be positioned in these regions before exposure to IL1B, which remained to be explained.

Note that there was no evidence for footprints in peaks adjacent to downregulated genes (data not shown). And the search for de *novo* motifs in ATAC-Seq peaks located near « ALL » or « UP » differentially genes did not reveal statistically relevant motif associated with *bona fide* average footprints (data not shown).

Constitutive expression of genes of the immune and inflammatory pathways at early stages of OPC maturation trajectory, in unstressed conditions

At this step of the study, we had shown that P5 O4+ OPCs were able to induce the expression of genes belonging to the immune system and inflammatory response pathways, in response to IL1B,

and that this was not due to contamination by other cell types. We had also shown that these major alterations in gene expression mainly occurred without overt modifications in chromatin accessibility, but that these open regions were bound in the PBS and IL1B conditions by key TFs controlling these pathways. This suggests that, because these IL1B-induced genes are already in an open chromatin conformation before IL1B exposure and constitutively bound by these TFs, they might be already physiologically transcribed in OPCs in control (unstressed) conditions and boosted by IL1B.

We MACS-isolated O4+ OPCs at P3, P5, and P10 and showed that, indeed, O4+ OPCs expressed reproducible cytokine and chemokine mRNA levels in normal conditions, which decreased in a stage-dependent manner, between P3 and P10 (Fig. 7*A* and Fig. S7*A*). First, we verified that PBS intraperitoneal injections did not constitute a stress, *per se*, that would induce the expression of cytokine and chemokine genes, even in the absence of IL1B administration. By comparing MACS-isolated O4+ OPCs from naïve, PBS-treated, or IL1B treated pups at P5, we observed that naïve and PBS-treated O4+ OPCs displayed similar levels of cytokine and chemokine gene expression at P5, in RT-qPCR experiments (Fig. S7*B*), showing that PBS injection was not responsible for constitutive cytokine and chemokine mRNA levels at P5. In contrast, IL1B-treated OPCs exhibited elevated levels of cytokine and chemokine mRNAs compared to naïve PBS OPC samples, as expected (Fig. S7*B*). In addition, we confirmed that the constitutive expression of cytokines and chemokines also occurred in normal condition, in the murine oligodendrial cell line, Oli-neu, (Fig. 7*B*) and showed that this constitutive expression decreased during Oli-neu differentiation, as was observed along the O4+ OPCs maturation trajectory (Fig. 7*B* and Fig. S7*C*). These data demonstrated that O4+ OPCs can intrinsically transcribe cytokine and chemokine genes at early OPC stages (P3), and that the expression of these genes is gradually downregulated during their maturation process between P3 and P10, in a physiological and developmental manner. This constitutive transcription is in line with the open chromatin status of these genes that we observe at P5 (Fig. S2*D*).

To further challenge our data, we performed data mining analyses, using an ATAC-Seq public dataset of human aortic endothelial cells (HAECs), isolated from aortic trimmings of donor hearts, and treated or not with IL1B (12; "HAEC dataset"; NCBI Gene Expression Omnibus; accession no: GSE89970). First, HAEC peaks were matched to OPC peaks through gene annotations, by taking only those peaks located within ±2 kb of the TSS and annotated with a matching 1-to-1 gene orthologue, as described in Material and Methods. In total we were able to match 7,739 peaks, including 100 differential peaks from the HAEC dataset. We observed that the corresponding 100 O4+ OPC ATAC-Seq peaks, either from PBS or IL1B samples, did not significantly differ from the HAEC IL1B dataset, whereas they significantly differed from the HAEC control dataset (Fig. 7*C*; Fig. S7*C*; Table S10). This indicated that, not only our OPC IL1B-exposed samples, but also our PBS samples harbored an "IL1B signature". These data mining analyses therefore provide additional evidence that, even in normal conditions, O4+ OPCs display chromatin features which resemble to that of cells exposed to IL1B, reinforcing the validity of our findings about cytokine and chemokine gene expression in unstressed and stressed O4+ OPCs.

DISCUSSION

Overall, our results indicate that the remarkable immunomodulatory capacities of premyelinating O4+ OPCs constitute one route of entry for the impact of neuroinflammation on OPC maturation, with limited effects on chromatin accessibility. Indeed, we observe that neuroinflammation mainly takes advantage of the presence of open chromatin regions corresponding to active transcriptional programs, of which the constitutive expression, in normal conditions, of genes of the immune and inflammatory pathways is the most prominent target for IL1B-induced disturbances.

The impact of IL1B exposure can thus be interpreted in the following way: by markedly increasing the levels of cytokine and chemokine gene expression at P3 and P5, IL1B produces a delay

in the normal downregulation of these genes at P5, and, therefore, maintains abnormally elevated levels of these players at this stage. This suggests that one major mechanism for IL1B-induced OPC maturation blockade operates by interfering with the normal stage-dependent expression and downregulation of players of the inflammation pathway, along the OPC maturation trajectory.

It has been extensively reported in the literature that OPCs and oligodendrocytes of the adult brain can express key players of immune and inflammatory processes, in pathological conditions. This includes studies of patients affected by multiple sclerosis (MS) or in *in vivo* models of experimental autoimmune encephalomyelitis (EAE; reviewed in 13). Here, we show that P5 O4+ OPCs synthesize key players of the inflammatory process in normal conditions, and, in that sense, display properties similar to that of adult OPCs and mature oligodendrocytes, that can shape the inflammatory environment. Our results are also in line with previous results showing that OPCs, derived *in vitro* from neurospheres, can activate cytokine genes in an EAE model (14). In a more original manner, we also unravel the physiological, constitutive expression of cytokine and chemokine genes in unstressed O4+OPCs at an early postnatal stage, P5. In line with our findings, Zeis et al. (13), by revisiting the microarray data sets by Cahoy et al. (15), pointed out the expression of genes belonging to the GO:term "immune system process", in PDGFRa+ unstressed OPCs, , which reinforces our data.

Only a limited number of genes belonging to the immune system and inflammatory pathways, and whose expression is dysregulated by IL1B, undergoes major changes in their chromatin landscape. Hypoxia-Inducible Factor 3, *Hif3a*, is one of them and was shown to be regulated, in an oxygen-independent manner, in two distinct models of inflammation, in non-neural cells (17,18). Interestingly, Cuomo et al. (18) established that proinflammatory cytokines are responsible for the activation of the *Hif3a* gene, through epigenetic changes and the involvement of NFkB. This suggests that some of the alterations of the chromatin landscape, which are driven by IL1B, might be secondary effects of the upregulation of proinflammatory cytokines that we identified as one major entry route for IL1B detrimental effects, *via* TFs that we pointed out as important for the upregulated expression of inflammatory players. Notably, hypoxia and inflammation share a large interface (19,20), and hypoxic conditions are also able to elicit DWMI (6).

Nevertheless, an attractive possibility is that the bulk of genes of the immune and inflammatory pathways, which show no major alteration in chromatin confirmation, could exhibit minor, but crucial differences in nucleosomal positioning that would correlate with major increase in transcription (positioning of the first nucleosome and phasing of the following ones). Such subtle modifications, but no major changes in chromatin accessibility, have been strikingly identified during ES cell differentiation along diverse cell lineages, for example (21).

Future studies will determine whether the restricted impact on neuroinflammation on chromatin accessibility in the premyelinating OPC reflects an intrinsic robustness of the epigenome. Alternatively, the epigenome might have been perturbed at earlier stages and have already recovered at P5. In both cases, the molecular basis underlying this robustness or recovery capacities remain to be explored.

Another question is the functional impact of the opening or closing of the chromatin in response to IL1B, in regions that we have identified by ATAC-Seq. As already mentioned, most of them do no correlate with major transcriptional changes. This could have two interpretations. The transcriptomic impacts of these epigenomic modifications might be "buffered"/minimized, thanks to the binding of different sets of TFs, which would deserve further investigations. Alternatively, TFs, which are multifaceted drivers, remodel the chromatin state and genome topology, often before changes in gene expression can be observed, as was demonstrated in studies on the molecular basis of cell fate (22). These modifications of the chromatin landscape could thus constitute an Achilles' heel for transcriptomic disturbances, that would occur either at later maturation stages, at temporal distance from the insult, or upon a second hit of neuroinflammation. The occurrence of additional inflammatory insults is relevant for the following reasons. Our model of neuroinflammation represents a moderate and chronic systemic inflammatory insult, clinically relevant in terms of impact on myelination and behavioral defects, and mimicking clinically silent or mild

chorioamnionitis observed in many preterm infants (7,8,10). However, besides exposure to prenatal inflammatory insults, preterm babies also face a heavy burden in terms of postnatal inflammatory insults (23). One exciting possibility is these TFs might also work at long-distance from the dysregulated genes, which would involve remodeling at multiple architectural levels (chromatin looping, TADs (tolopogically associated domains) connectivity etc.).

Besides these considerations, the entry route, which is represented by the constitutive and stage-dependent synthesis of cytokines and chemokines by premyelinating OPCs in normal conditions, and which empowers neuroinflammation to impact OPC maturation, can be envisioned as recapitulating and intermingling both injurious and developmental aspects, as already expected from the field (24). Indeed, by counteracting the tightly regulated physiological expression of cytokines and chemokines by O4+ OPCs at P3, that is programmed to gradually decrease in a developmental, stage-dependent manner at later stages (here shown between P3 and P10), the IL1B insult might compromises the premyelinating OPC cell fate. Moyon et al. (16) pointed out the role of IL1B and CCL2 production by premyelinating OPCs in their motility capacities and eventually differentiation (see also 25). In addition, this production could regulate the recruitment by OPCs of other cells (like microglia; 26,27) that are known to influence OPC maturation.

In conclusion, in the context of a chronic, mild perinatal systemic inflammation, the epigenome seems globally preserved in premylienating OPCs, in terms of chromatin accessibility, and the contribution to OPC blockade is mostly driven by transcriptomic disturbances, that target transcriptional programs already open at the time of exposure. Further studies focusing on the most prominent of these programs, the immune system and inflammatory pathways, and on the TFs that governs these pathways, should pave the way for early intervention.

LEGENDS OF FIGURES

Figure 1. Experimental strategy. Previously validated mouse model of encephalopathy of prematurity. IL1B is administered intra-peritoneally from postnatal days 1 to 5, which mimics neuroinflammatory insults as undergone by human fetuses in the third trimester of pregnancy, and their pathological consequences in terms of OPC maturation blockade, defective myelination, brain developmental, and behavioral anomalies (7). O4+ OPCs (green circles) were isolated from the cortices of newborn male OF1 pups by magnetic activated cell sorting at P5. Genome-wide chromatin accessibility was explored by ATAC-Seq on this purified OPC population (lower, left panel): the enzymatic severing of the DNA by the transposome (Tn5 transposase, loaded with adapters *in vitro*; green and orange) allows « tagmentation » of DNA template, to fragments tagged with adapters. In parallel (lower, right panel), comparative transcriptomic analysis was performed using Agilent mouse whole genome microarray.

Figure 2. The epigenome of OPCs is globally unchanged by IL1B treatment as assessed by ATAC-Seq analysis of chromatin accessibility.

A) PCA analysis of log normalized read counts falling within ATAC-seq chromatin peaks from OPCs upon PBS or ILB1B injections (total number of peaks: 213,246). Principal component 1 (PC1; x axis corresponds to 42% of the variance axis) and Principal component 2 (PC2; y axis corresponds to 24% of the variance).

(*B*) Scatter plot representing the dispersion of the variations (logFC; (FC, fold change)) induced by IL1B, as the number of *reads* (logCPM), for each individual analyzed peak (3 PBS samples and 3 IL1B samples). In red, the 524 peaks differentially showing increased (391 peaks) or decreased (134 peaks) chromatin accessibility with FDR < 0.05.

(*C*) Heat map visualization of the 524 open (yellow) or closed (blue) peaks in PBS and IL1B conditions.

(*D*) Examples of peaks showing increased chromatin accessibility: (Upper and middle panels) peak located at the most downstream position in the *Hif3a gene* (*Hypoxia inducible factor 3 alpha subunit;* magnification in the middle panel). Example of peak with non-significant changes in chromatin accessibility: (Upper panel) the peak located in the middle of the *Hif3a* gene illustrated region. Example of peak showing reduced chromatin accessibility: peaks within the *Cwc22* gene (encoding the spliceosome-associated protein 22).

Figure 3. Gene of the immune system and inflammatory response pathway represents the top 5 most upregulated genes, upon IL1B treatment. Microarray analysis comparing gene expression in isolated O4+ OPCs from 6 independent control (PBS) and 6 independent IL1B-exposed cortices (IL1B; Fig. 1).

(*A*) **Heat map of the genes whose expression is disturbed by IL1B exposure.** A fold-change (FC) threshold of +/-1.5 was chosen, with FDR < 0.05. Total number of probes corresponding to IL1B-induced disturbances in gene expression: 2571, corresponding to 1719 genes. Total number of probes corresponding to the 1266 upregulated genes: 1872. Total number of probes corresponding to the 454 downregulated genes: 699 (some genes are represented by more than one probe). Heatmap color scale: log2 [-2.0;+2.0].

(*B*) **Quality control of the samples used for microarray analysis.** Microarray analysis of FC in gene expression of myelin markers that start to be expressed at P5 and of OPC markers.

(*C*) **RT-qPCR analysis of the expression of myelination and progenitor markers in OPCs**.

Myelin markers: *Mbp*, Myelin binding protein; *Mog*, Myelin oligodendrocyte glycoprotein; *Mag*, Myelin-associated glycoprotein. *Plp1*, proteolipid protein 1, a transmembrane, predominant component of myelin; *Cnp*, 2',3'-Cyclic Nucleotide 3' Phosphodiesterase, abundant protein in myelin in the central nervous system. Progenitor (OPC) markers: *Id2*, Inhibitor of differentiation 2; *Pdgfra*, Platelet Derived Growth Factor Receptor Alpha, a marker of OPCs. Number of independent experiments: n = 7 for *Cnp*, *Mag*, and *Pdgfra*; and n = 15 for *Mbp*, *Mog*, and *Id2*. ns: not statistically significant; * p < 0.05; *** p< 0.001.

(*D*) **The Top5 GO of up-regulated genes corresponds to the immune system and inflammatory**

response pathways.
(*E*) **Heat map of the genes belonging to the Top5 GO, whose expression is disturbed by IL1B exposure** (315 probes corresponding to 262 genes). Heatmap color scale: log2 [-2.0;+2.0].
(*F*) **RT-qPCR analysis of the gene expression of players of the GO "immune system and inflammatory response pathways" in O4+ OPCs**. Number of independent experiments: n =8 for all genes, except for *Cxcl9*, *Cxcl10*, and *Il1r1* (n=7).* $p < 0.05$; ** $p< 0.01$; *** $p< 0.001$.

Figure 4. The induction in cytokine and chemokine expression by IL1B in OPCs at P5 is not due to contamination by microglial cells (CD11+) or astrocytes (GLAST+)
(*A*) Overexpression of the 262 genes of the inflammatory pathway is observed in isolated O4+ OPCs, in contrast to CD11+ microglial cells (8) in microarrays analyses at P5.
(*B*) Fold-change in gene expression in isolated O4+ OPCs, CD11+ microglial cells, and GLAST+ astrocytes. Time-course RT-qPCR analysis at P1, P5, and P10. mRNA levels are normalized to *Gapdh* for OPCs and astrocytes and *Rpl13* for microglia. The numbers of independent experiments are indicated on each plot. For OPCs, n=5 at P1; n= 8 at P5; n= 11 at P10 (except for *Cxcl1*, n =10). For microglia, n= 4 at P1; n=3 at P3; n= 6 at P5; n= 5 at P10. For astrocytes n =4 for each time point and each gene. * $p < 0.05$; ** $p< 0.01$; *** $p< 0.001$.

Figure 5. The production of cytokine and chemokine proteins is induced by IL1B in MACS-isolated O4+ OPCs, cultured *ex vivo*
(*A*) Experimental design for *ex vivo* OPC culture, treatment, and differentiation.
(*B*) Detection and quantification (pG/mL) of the expression of interleukins (IL1B, IL6), cytokine C-C Motif Chemokine Ligand 2, 4, and 5 proteins (CCL2, CCL3, CCL4, and CCL5) and chemokine C-X-C Motif Chemokine Ligand 2 (CXCL2) proteins by Luminex. The dotted line represents the limit of detection for individual proteins in the assay. The numbers of independent experiments performed for each plot are indicated on each plot. * $p < 0.05$; ** $p< 0.01$; *** $p< 0.001$.

Figure 6. Crossing of ATAC-Seq and microarray data reveals major involvement of TFs of the immune and inflammatory pathways.
(*A*) Number of genes differentially expressed upon ILB exposure and associated with differentially accessible peaks/regions.
(*B*) Number of genes differentially expressed upon ILB exposure and associated with differentially accessible peaks/regions located +/- 8 kb around their TSS.
(*C*) **Heatmap illustrating the co-localization of pairs of TF binding motif**s identified by the paired motif analysis in the 2319 ATAC-Seq peaks located into +/- 8 kb around the 1266 upregulated genes (corresponding to 886 different gene names). TF names from MEME nomenclature on both axes. Statistically relevant co-occurrence of two different TFs is indicated by yellow to orange squares (log10 p-value adjusted). Examples of TF pairs are indicated IRF1-p50; *ISRE*-p65; PU.1-IRF8-p65; PU.1-iRF8-p50; PU.1-BATF; PU.1-FOSL2. Red lines: pairing of PU.1-IRF8 with NFKB subunit binding motifs. Purple lines: pairing of PU.1-IRF8 with AP-1 family binding motifs. Blue lines: pairing of NFKB binding motifs with *Isre* (IFN-stimulated response element). Green lines: Pairing of NFKB with IRF binding motifs.
(*D*) **Examples of chromatin accessibility footprints at TF motifs:** average footprint profiles at TF motifs were plotted at base pair resolution, located within accessible chromatin *loci* in <u>both</u> PBS and ILB conditions, adjacent to differentially regulated genes (ALL; down and upregulated) using the Wellington software. Typical footprint profiles coincide with the center of the canonical motif for a given TF (indicated by brackets). Footprints for occupancy of IRF1, IRF2, *Isre,* and NFκB binding motifs are illustrated. Red and blue curves: + and - strand, respectively.

Figure 7. Constitutive expression of genes encoding cytokines and chemokines at early stages of normal (unstressed) O4+ OPC maturation.

(*A*) RT-qPCR analyses in P3, P5, and P10 O4+ OPCs. N= 5 to 6 independent experiments. Two-way ANOVA followed by Bonferroni - Post Hoc Test was performed: * et + $p < 0.05$; ** et ++ $p< 0.01$; *** $p< 0.001$. *, **, or *** correspond to comparison between PBS and IL1 conditions for a given postnatal stage; + or ++ correspond to comparison between P5 (or P10) to P3.
(*B*) RT-qPCR analyses in the Oli-neu cell line before or after 72 hours of differentiation triggered by PD174265, a potent, cell-permeable inhibitor of the tyrosine kinase activity of the epidermal growth factor receptor (EGFR). Numbers of independent experiments are indicated on the graph bars. * $p < 0.05$; ** $p< 0.01$. nd: not detected.
(*C*) **Comparison of 100 human HAEC differential peaks matched with mouse OPC peaks.** Read number distribution of peaks upon IL1B treatment in the HAEC and OPC datasets. Reads were normalized for each set of peaks against the total number of reads present in all (7,739) matched peaks and converted into reads per million.

LEGENDS OF SUPPLEMENTAL FIGURES

Figure S1. (related to Fig. 1).
(*A*) **Quality assessment of the O4+ OPC cell purification process**. RT-qPCR experiments on the O4+ OPC, CD11+ microglia (8), (3 PBS samples and 3 IL1B samples) and unlabelled cell populations, showing that, in contrast to microglia and astrocytes (unlabelled), O4+ OPCs, used in this study, express the *Mbp* gene, but very low mRNA levels of the microglia marker CD11 (encoded by the *Itgam* gene), the astrocyte marker *Gfap*, or of the neuronal marker *NeuN*. Note that *NeuN* is very lowly expressed, even in the unlabelled population, which mainly contains astrocytes, because neurons poorly survive our MACS protocol.
(*B*) **Schematic representation of the bioinformatics and statistics workflow used for the analysis of ATAC-Seq data**
(C) **ATAC-Seq resolved nucleosome profiles**. Insert size distribution shows visible large periodicity of the nucleosome-free, mononucleosomal and dinucleosomal fragments, as well as the expected ~10.4bp periodicity, resulting from steric hindrance of the helical twist of the DNA.

Figure S2. The epigenome of OPCs is globally unchanged by IL1B treatment as assessed by ATAC-Seq analysis of chromatin accessibility (related to Fig. 2).
(*A*) Multidimentional Scaling (MDS) Plot of distances between the 3 PBS samples and the 3 IL1B samples, using EdgeR.
(*B*) Scatter plots representing the dispersion of the variations (logFC; (FC, fold change)) as the number of *reads* (logCPM), for each individual analyzed peak (3 PBS samples and 3 IL1B samples). In red, peaks showing differential chromatin accessibility with FDR < 0.05. Note that the upper plot located on the left is identical to the one in Fig 2*B* but was also put in this Fig. S2, for easier comparison with the other plots. Upper right, lower left, and lower right: scatter plots for simulated data sets, created by swapping of one of the PBS samples with one other IL1B samples or, vice-versa. Mixing PBS and IL-1B samples led to very reduced number of peaks differentially open or closed, indicated that OPC treatment by IL1B is responsible for the appearance of differentially open and closed peaks.
(C) Distribution of the total number of peaks (upper panel) or of the 524 differential open or closed peaks (lower panel) in various genomic regions.
(*D*) Examples of peaks showing reduced or unchanged chromatin accessibility: the cytokine C-C Motif Chemokine Ligand 2 gene (*Ccl2*; upper panel), or *C-X-C Motif Chemokine Ligand 1* and *10* genes *(Cxcl1* or *Cxcl10; Lower panels)*, respectively.
(*E*) GO analysis, using DAVID6.8, corresponding to the TOP-10 genes, whose TSS is located the closest to the 524 ATAC-Seq peaks showing differentially chromatin accessibility, upon IL1B treatment.

Figure S3. GO analysis corresponding to the TOP-10 genes, downregulated upon IL1B treatment, using DAVID6.8 (related to Fig. 3).

Figure S4. Heat maps of the overall comparison of IL1B-induced perturbations in gene expression in isolated O4+ OPCs and CD11+ microglial cells. (related to Fig. 4). OP4+ OPCs exhibit profiles of transcriptomic modifications globally very different from that of CD11+ microglial cells. Examples of genes encoding cytokines and chemokines are pointed out by rectangles. Most of them are not upregulated in CD11+ microglial cells at P5, in contrast to what happens in O4+ OPCs. Fold change ([-2.0; +2.0]; IL1B/PBS).

Figure S5. (related to Fig. 5 and Fig. 6).
(*A*) **The induction of cytokine and chemokine mRNA levels, upon IL1B exposure, is reproduced in MACS-isolated *ex vivo* cultured OPCs during differentiation**. RT-qPCR experiments on OPCs collected after 72h of differentiation. Number of independent experiments: n = 6 per condition (PBS or IL1B). * $p < 0.05$; ** $p < 0.01$; *** $p < 0.01$.

(*B*) TFBS motifs identified in significant ATAC-seq peaks adjacent to differentially regulated genes, using HOMER known motifs.
(*C*) TFBS motifs identified in significant ATAC-seq peaks adjacent to upregulated genes, using HOMER known motifs.

Figure S6. Examples of chromatin accessibility footprint profiles at TF motifs. (related to Fig. 6). Average footprint profiles at TF motifs plotted at base pair resolution, located within accessible chromatin *loci* adjacent to any differentially regulated genes (ALL; down or upregulated), in the following samples: PBS-treated only, IL1B-treated-only, or from both conditions (PBS plus IL1B): IRF1, IRF2, *Isre,* NFκB, PU.1-IRF8, PGR.

Figure S7. Constitutive expression of cytokines and chemokines by unstressed early maturating OPCs and subsequent decrease. (related to Fig. 7).

(*A*) RT-qPCR analyses in P3, P5, and P10 O4+ OPCs showing the expected increase in the expression of genes associated with myelination between P5 and P10 in normal conditions and expected impairment of this increase upon IL1B exposure. Note that in this set of experiments the downregulation of myelination genes was not observed at P5, a stage at which these genes only start to be expressed.
(*B*) RT-qPCR experiments comparing O4+ OPC from naïve (no injection), PBS-injected and IL1B-injected pups, showing that PBS injection does not induce expression of cytokines and chemokine genes, since transcripts levels are equivalent in both PBS and naïve conditions, in contrast to what is observed upon IL1B treatment.
(*C*) RT-qPCR analyses in the Oli-neu cell line before or after 72 hours of differentiation triggered by exposure to conditioned medium from primary neuron culture.
(*D*) **Comparison of all the matched peaks between the Hogan and Paris datasets.** Read number distribution of peaks upon IL1B treatment in the HAEC and OPC datasets. Reads were normalized for each set of peaks against the total number of reads present in the 7739 matched peaks and converted into reads per million (RPM).

REFERENCES

1. Ball G, Boardman JP, Rueckert D, Aljabar P, Arichi T, Merchant N, Gousias IS, Edwards AD, Counsell SJ. The effect of preterm birth on thalamic and cortical development. Cereb Cortex. 2012 May;22(5):1016-24. doi: 10.1093/cercor/bhr176. PMID: 21772018

2. Billiards SS, Haynes RL, Folkerth RD, Borenstein NS, Trachtenberg FL, Rowitch DH, Ligon KL, Volpe JJ, Kinney HC. Myelin abnormalities without oligodendrocyte loss in periventricular leukomalacia. Brain Pathol. 2008 Apr;18(2):153-63. doi: 10.1111/j.1750-3639.2007.00107.x. PMID: 18177464

3. Delobel-Ayoub M, Arnaud C, White-Koning M, Casper C, Pierrat V, Garel M, Burguet A, Roze JC, Matis J, Picaud JC, Kaminski M, Larroque B; EPIPAGE Study Group. Behavioral problems and cognitive performance at 5 years of age after very preterm birth: the EPIPAGE Study. Pediatrics. 2009 Jun;123(6):1485-92. doi: 10.1542/peds.2008-1216. PMID: 19482758

4. Nelson KB, Dambrosia JM, Grether JK, Phillips TM. Neonatal cytokines and coagulation factors in children with cerebral palsy. Ann Neurol. 1998 Oct;44(4):665-75. PMID: 9778266

5. Leviton A, Gressens P. Neuronal damage accompanies perinatal white-matter damage. Trends Neurosci. 2007 Sep;30(9):473-8. PMID: 17765331

6. Hagberg H, Mallard C, Ferriero DM, Vannucci SJ, Levison SW, Vexler ZS, Gressens P. The role of inflammation in perinatal brain injury. Nat Rev Neurol. 2015 Apr;11(4):192-208. doi: 10.1038/nrneurol.2015.13. PMID: 25686754

7. Favrais G, van de Looij Y, Fleiss B, Ramanantsoa N, Bonnin P, Stoltenburg-Didinger G, Lacaud A, Saliba E, Dammann O, Gallego J, Sizonenko S, Hagberg H, Lelièvre V, Gressens P. Systemic inflammation disrupts the developmental program of white matter. Ann Neurol. 2011 Oct;70(4):550-65. doi: 10.1002/ana.22489. PMID: 21796662

8. Krishnan ML, Van Steenwinckel J, Schang AL, Yan J, Arnadottir J, Le Charpentier T, Csaba Z, Dournaud P, Cipriani S, Auvynet C, Titomanlio L, Pansiot J, Ball G, Boardman JP, Walley AJ, Saxena A, Mirza G, Fleiss B, Edwards AD, Petretto E, Gressens P. Integrative genomics of microglia implicates DLG4 (PSD95) in the white matter development of preterm infants. Nat Commun. 2017 Sep 5;8(1):428. doi: 10.1038/s41467-017-00422-w. PMID: 28874660

9. Buenrostro JD, Giresi PG, Zaba LC, Chang HY, Greenleaf WJ. Transposition of native chromatin for fast and sensitive epigenomic profiling of open chromatin, DNA-binding proteins and nucleosome position. Nat Methods. 2013 Dec;10(12):1213-8. doi: 10.1038/nmeth.2688. PMID: 24097267

10. Volpe JJ. Brain injury in premature infants: a complex amalgam of destructive and developmental disturbances. Lancet Neurol. 2009 Jan;8(1):110-24. doi: 10.1016/S1474-4422(08)70294-1. PMID: 19081519

11. Piper J, Elze MC, Cauchy P, Cockerill PN, Bonifer C, Ott S. Wellington: a novel method for the accurate identification of digital genomic footprints from DNase-seq data. Nucleic Acids Res. 2013 Nov;41(21):e201. doi: 10.1093/nar/gkt850. Epub 2013 Sep 25. Erratum in: Nucleic Acids Res. 2014;42(17):11272. PMID: 24071585

12. Hogan NT, Whalen MB, Stolze LK, Hadeli NK, Lam MT, Springstead JR, Glass CK, Romanoski CE. Transcriptional networks specifying homeostatic and inflammatory programs of gene expression in

human aortic endothelial cells. Elife. 2017 Jun 6;6. pii: e22536. doi: 10.7554/eLife.22536. PMID: 28585919

13. Zeis T, Enz L, Schaeren-Wiemers N. The immunomodulatory oligodendrocyte. Brain Res. 2016 Jun 15;1641(Pt A):139-148. doi: 10.1016/j.brainres.2015.09.021. Epub 2015 Sep 28. PMID: 26423932

14. Kang Z, Wang C, Zepp J, Wu L, Sun K, Zhao J, Chandrasekharan U, DiCorleto PE, Trapp BD, Ransohoff RM, Li X. Act1 mediates IL-17-induced EAE pathogenesis selectively in NG2+ glial cells. Nat Neurosci. 2013 Oct;16(10):1401-8. doi: 10.1038/nn.3505. Epub 2013 Sep 1. PMID: 23995070

15. Cahoy JD, Emery B, Kaushal A, Foo LC, Zamanian JL, Christopherson KS, Xing Y, Lubischer JL, Krieg PA, Krupenko SA, Thompson WJ, Barres BA. A transcriptome database for astrocytes, neurons, and oligodendrocytes: a new resource for understanding brain development and function. J Neurosci. 2008 Jan 2;28(1):264-78. doi: 10.1523/JNEUROSCI.4178-07.2008. PMID: 18171944

16. Moyon S, Dubessy AL, Aigrot MS, Trotter M, Huang JK, Dauphinot L, Potier MC, Kerninon C, Melik Parsadaniantz S, Franklin RJ, Lubetzki C. Demyelination causes adult CNS progenitors to revert to an immature state and express immune cues that support their migration. J Neurosci. 2015 Jan 7;35(1):4-20. doi: 10.1523/JNEUROSCI.0849-14.2015. PMID: 25568099

17. Kumar H, Lim JH, Kim IS, Choi DK. Differential regulation of HIF-3α in LPS-induced BV-2 microglial cells: Comparison and characterization with HIF-1α. Brain Res. 2015 Jun 12;1610:33-41. doi: 10.1016/j.brainres.2015.03.046. Epub 2015 Apr 3. PMID: 25847716

18. Cuomo F, Coppola A, Botti C, Maione C, Forte A, Scisciola L, Liguori G, Caiafa I, Ursini MV, Galderisi U, Cipollaro M, Altucci L, Cobellis G. Pro-inflammatory cytokines activate hypoxia-inducible factor 3α via epigenetic changes in mesenchymal stromal/stem cells. Sci Rep. 2018 Apr 11;8(1):5842. doi: 10.1038/s41598-018-24221-5. PMID: 29643458

19. Bartels K, Grenz A, Eltzschig HK. Hypoxia and inflammation are two sides of the same coin. Proc Natl Acad Sci U S A. 2013 Nov 12;110(46):18351-2. doi: 10.1073/pnas.1318345110. PMID: 24187149

20. Scholz CC, Cavadas MA, Tambuwala MM, Hams E, Rodríguez J, von Kriegsheim A, Cotter P, Bruning U, Fallon PG, Cheong A, Cummins EP, Taylor CT. Regulation of IL-1β-induced NF-κB by hydroxylases links key hypoxic and inflammatory signaling pathways. Proc Natl Acad Sci U S A. 2013 Nov 12;110(46):18490-5. doi: 10.1073/pnas.1309718110. Epub 2013 Oct 21. PMID: 24145445

21. West JA, Cook A, Alver BH, Stadtfeld M, … Park PJ, Tolstorukov MY, Kingston RE. Nucleosomal occupancy changes locally over key regulatory regions during cell differentiation and reprogramming. Nat Commun 2014 5:4719. PMID: 25158628.

22. Stadhouders R, Vidal E, Serra F, Di Stefano B, Le Dily F, Quilez J, Gomez A, Collombet S, Berenguer C, Cuartero Y, Hecht J, Filion GJ, Beato M, Marti-Renom MA, Graf T. Transcription factors orchestrate dynamic interplay between genome topology and gene regulation during cell reprogramming. Nat Genet. 2018 Feb;50(2):238-249. doi: 10.1038/s41588-017-0030-7. Epub 2018 Jan 15. PMID: 29335546

23. Barnett ML, Tusor N, Ball G, Chew A, Falconer S, Aljabar P, Kimpton JA, Kennea N, Rutherford M, David Edwards A, Counsell SJ. Exploring the multiple-hit hypothesis of preterm white matter damage using diffusion MRI. Neuroimage Clin. 2017 Nov 21;17:596-606. doi: 10.1016/j.nicl.2017.11.017. eCollection 2018. PMID: 29234596

24. Volpe JJ. Systemic inflammation, oligodendroglial maturation, and the encephalopathy of prematurity. Ann Neurol. 2011 Oct;70(4):525-9. doi: 10.1002/ana.22533. PMID: 22028217

25. Vela JM1, Molina-Holgado E, Arévalo-Martín A, Almazán G, Guaza C. Interleukin-1 regulates proliferation and differentiation of oligodendrocyte progenitor cells. Mol Cell Neurosci. 2002 Jul;20(3):489-502. PMID: 12139924

26. Jana M, Pahan K. Redox regulation of cytokine-mediated inhibition of myelin gene expression in human primary oligodendrocytes. Free Radic Biol Med. 2005 Sep 15;39(6):823-31. PMID: 16109311

27. Balabanov R, Strand K, Goswami R, McMahon E, Begolka W, Miller SD, Popko B. Interferon-gamma-oligodendrocyte interactions in the regulation of experimental autoimmune encephalomyelitis. J Neurosci. 2007 Feb 21;27(8):2013-24. PMID: 17314297

28. (or Suppl. Reference) Schang AL, Van Steenwinckel J, Chevenne D, Alkmark M, Hagberg H, Gressens P, Fleiss B. Failure of thyroid hormone treatment to prevent inflammation-induced white matter injury in the immature brain. Brain Behav Immun. 2014 Mar;37:95-102. doi: 10.1016/j.bbi.2013.11.005. Epub 2013 Nov 12. PMID: 24240022

29. McCarthy KD, de Vellis J. Preparation of separate astroglial and oligodendroglial cell cultures from rat cerebral tissue. J Cell Biol. 1980 Jun;85(3):890-902. PMID: 6248568

30. Pansiot J, Pham H, Dalous J, Chevenne D, Colella M, Schwendimann L, Fafouri A, Mairesse J, Moretti R, Schang AL, Charriaut-Marlangue C, Gressens P, Baud O. Glial response to 17 β-estradiol in neonatal rats with excitotoxic brain injury. Exp Neurol. 2016 Aug;282:56-65. doi: 10.1016/j.expneurol.2016.05.024. Epub 2016 May 21. PMID: 27222132

31. Jung M, Krämer E, Grzenkowski M, Tang K, Blakemore W, Aguzzi A, Khazaie K, Chlichlia K, von Blankenfeld G, Kettenmann H, et al. Lines of murine oligodendroglial precursor cells immortalized by an activated neu tyrosine kinase show distinct degrees of interaction with axons in vitro and in vivo. . Eur J Neurosci. 1995 Jun 1;7(6):1245-65. PMID: 7582098

32. Gobert RP, Joubert L, Curchod ML, Salvat C, Foucault I, Jorand-Lebrun C, Lamarine M, Peixoto H, Vignaud C, Frémaux C, Jomotte T, Françon B, Alliod C, Bernasconi L, Abderrahim H, Perrin D, Bombrun A, Zanoguera F, Rommel C, Hooft van Huijsduijnen R. Convergent functional genomics of oligodendrocyte differentiation identifies multiple autoinhibitory signaling circuits. Mol Cell Biol. 2009 Mar;29(6):1538-53. doi: 10.1128/MCB.01375-08. Epub 2009 Jan 12. PMID: 19139271

33. Robinson MD, McCarthy DJ, Smyth GK (2010). "edgeR: a Bioconductor package for differential expression analysis of digital gene expression data." Bioinformatics **26**(1), 139-140. PMID: 19910308

34. Huang da W, Sherman BT, Lempicki RA. Systematic and integrative analysis of large gene lists using DAVID bioinformatics resources. Nat Protoc. 2009;4(1):44-57. doi: 10.1038/nprot.2008.211. PMID: 19131956

35. Huang da W, Sherman BT, Lempicki RA. Bioinformatics enrichment tools: paths toward the comprehensive functional analysis of large gene lists. Nucleic Acids Res. 2009 Jan;37(1):1-13. doi: 10.1093/nar/gkn923. Epub 2008 Nov 25. PMID: 19033363

36. Chhor V, Le Charpentier T, Lebon S, Oré MV, Celador IL, Josserand J, Degos V, Jacotot E, Hagberg H, Sävman K, Mallard C, Gressens P, Fleiss B. Characterization of phenotype markers and

neuronotoxic potential of polarised primary microglia in vitro. Brain Behav Immun. 2013 Aug;32:70-85. doi: 10.1016/j.bbi.2013.02.005. Epub 2013 Feb 27. PMID: 23454862

37. Green B, Bouchier C, Fairhead C, Craig NL, Cormack BP. Insertion site preference of Mu, Tn5, and Tn7 transposons. Mob DNA. 2012 Feb 7;3(1):3. doi: 10.1186/1759-8753-3-3. PMID: 22313799

MATERIAL AND METHODS

Animal Model

Experimental protocols were approved by the institutional review committee and met the guidelines for the United States Public Health Service's Policy on Humane Care and Use of Laboratory Animals (NIH, Bethesda, MD, USA). Sex was determined at birth, and confirmed by abdominal examination at sacrifice. To avoid any potential variability linked to sex differences, only male OF1 pups were used. IL1B injections were performed as described (7,8. Five µL volume of phosphate-buffered saline (PBS) containing 10µG/kG/injection of recombinant mouse IL1B (R&D Systems, Minneapolis, MN) or of PBS alone (control) was injected intraperitoneally (i.p.) twice a day on days P1 to P4 and once a day on day P5 (see Fig. 1). Pups were sacrificed four hours after the morning injection of IL1B at P3, P5, P9, or P10. ATAC-Seq data were produced from 3 independent biological replicates for each condition (PBS or IL1B; Fig. 1). Microarray data were produced from 6 independent biological replicates for each condition (PBS or IL1B; Fig. 1), using the same animals that were also analysed for CD11+ microarrays (8).

O4+ magnetic and microglial activated cell sorting in mouse

O4+ cells were isolated at P3, P5, P9, or P10 by Magnetic Activated Cell Sorting (MACS, Miltenyi Biotec, Bergisch Gladbach, Germany), according to the manufacturer's protocol and as previously described (28). Briefly, brains were collected without cerebellum and olfactory bulbs, pooled (3 brains per sample) and dissociated using the Neural Tissue Dissociation Kit containing papain. O4 + cells were then enriched by MACS, using the anti-O4 MicroBeads. For microarray and RT-qPCR analysis, the eluted isolated cells were centrifuged for 5 min at 600g and conserved at -80°C. CD11+ microglial cells were isolated as described (8). The unlabelled fraction mainly contained astrocytes (see Fig. S1*A*). For the ATAC-seq experiment, 50,000 cells were immediately lysed and their nuclei submitted to Tn5 activity. The purity of the eluted O4-positive fraction was verified using qRT-PCR for Myelin Basic Protein (*Mbp*), ionizing calcium binding adapter protein (*Iba1*), glial fibrillary acid protein (*Gfap*) and neuronal nuclear antigen mRNAs (*NeuN*; Fig. S1*A*).

OPC culture and differentiation

OPCs were prepared from newborn OF1 mice as described (29,30). In brief, forebrain cortices were removed from postnatal day 0–2 mouse pups and freed from meninges. Minced tissues were enzymatically digested with 0.125% trypsin (Sigma) and 0,0025% DNase I (Sigma) for 15 min at 37C and then mechanically dissociated. Cells were filtered through a 100-µm-pore-size cell strainer (BD), centrifuged 10 min at 1800 rpm, resuspended in minimum essential Eagle's medium (Sigma) supplemented with 10% FBS (Gibco), 1% Glutamax (Gibco), 1% penicillin-streptomycin (P/S) solution (Sigma), and 0.5% glucose and plated in T75 flasks at a density of $2 \times 10^5/cm^2$. Mixed glial cell cultures were grown until confluence for 9-11 days (medium was renewed every 48-72h) and shaken for 1.5 h at 260 rpm to remove microglia. Remaining cells were shaken for additional 18h to detach the OPCs from astrocytes, and were simultaneously treated with 100 µg/ml liposomal clodrosome suspension (Clodrosome®, Encapsula Nanosciences, Brentwood, USA) which selectively eliminates microglia. Cell suspension was filtered through a 20-µM-pore-size filter (Millipore) and incubated in an untreated Petri dish for 10 min at 37°C to allow attachment of remaining microglia. Purified OPCs were seeded onto poly-D-lysine-coated 12-multiwell plates at a density of $3 \times 10^4/cm^2$ in OPC proliferation medium composed of Neurobasal medium (Gibco), 2% B21 (Miltenyi biotec), 1% P/S (Sigma) and 1% Glutamax (Gibco), supplemented with growth factors consisting in 10nG/mL FGFα (Sigma) and 10nG/mL PDGFα (Sigma). After 72h, OPC differentiation was initiated by growth factor withdrawal and addition of 40 nG/mL de T3 (Sigma). At the same time, cells were treated with 50nG/mL IL1B (R&D Systems, Minneapolis, MN) or PBS during 4h, treatment was removed and cells were grown in differentiation medium until 72h (Fig. 5*A*).

Oli-neu cell line culture and differentiation

The immortalized murine OPC cell line, Oli-neu, was kindly provided by Dr Sheila Harroch (Pasteur Institute, Paris, France). Oli-neu was established from OPC-enriched murine primary cultures from E16 brains transformed with a provirus containing the oncogene *T-Neu* (31). Various differentiation protocols have been established, among which treatment with PD174265, a selective inhibitor of the activity of Epidermal Growth Factor receptor (ErbB) tyrosine kinase, has been shown to induce MBP expression (32). These cells were cultured in Dulbecco's modified Eagle's minimum essential medium (DMEM) containing Glutamax 1X and high glucose (4.5 G/L) (Gibco 31966), supplemented with 1 mG/mL insulin (Sigma), N2 supplement (Gibco), 100 µG/mL T4 and T3 (Sigma), 1% horse serum (Gibco), and 1% P/S (Sigma). At confluence, the cells were mechanically detached and seeded in 12-multiwell plates at a density of 15,000 cells/cm². After 24h, differentiation was induced by addition of 1µM PD174265 (ChemCruz) previously diluted in DMSO at 1 mM. Medium was renewed after 48h and differentiation was stopped after 72h. Another differentiation protocol using one third of conditioned medium from primary neuronal culture (36; Fig. S7*C*).

ATAC-Seq analysis in O4+ OPCs

ATAQ-seq protocol was realized as described initially with slight modifications (9). In brief, cells were immediately lysed after cell sorting and a total of 50,000 nuclei were subjected to Tn5-mediated transposition for 30 min. Tagmented DNA was purified on MinElute colums (Qiagen) and amplified/tagged in two steps using NEBnext High-Fidelity 2x PCR master mix (New England Biolabs). Amplified DNA was purified twice with 1.8 volumes of NucleoMag NGS Clean-up and Size Select beads (Macherey Nagel). DNA was quantified using the Qubit dsDNA HS Assay Kit and the quality of each library determined on Agilent 2100 Bioanalyzer DNA High Sensitivity ChIPs. Libraries demonstrating appropriate nucleosomal profiles were multiplexed and subjected to Illumina NextSeq sequencing (IGenSeq Platform, ICM, Paris, France). Fastq files are available in Dataset S1. The main steps of sequence analyses are summarized in Fig. S1*B*. After quality controls (Fastqc and Trimmomatic 0.33), reads were aligned on the mm10 genome with Bowtie 2 (Galaxy tool version 2.3.4.1; default parameters) (Table S1; Fig. S1*B*). Peak calling was performed with MACS2.2.0; default parameters; q<0,05) separately for the two conditions, using a pooled (n=3) bam file of control samples and a pooled (n=3) bam file of IL1B samples. The two resulting bed files were merged and, after removing the mm10 blacklist (http://mitra.stanford.edu/kundaje/akundaje/release/blacklists/mm10-mouse/mm10.blacklist.bed.gz), 213,245 DNA regions (peaks) significantly detected in at least one condition were delimitated (Table S2). The number of reads was determined in each peak for each sample using Bedtools coverage (2.19.1) and normalized to the library sizes. Principal component analysis was performed on log transformed read count values of the top 500 most variable peaks, using the prcomp function in R. Differential peak detection between the 3 PBS and the 3 IL1B samples was performed with the Bioconductor software package EdgeR (3.22.3; 33) using R studio (0.98.1103; http://www.rstudio.com). Statistical comparison was performed using the exact test function followed by False discovery Rate (FDR) determination by the Benjamini-Hochberg method.

Crossing of HAEC and OPC ATAC-Seq datasets

We used a public of ATAC-Seq dataset of human aortic endothelial cells (HAECs; 12; NCBI Gene Expression Omnibus; accession no: GSE89970) and processed the raw reads (using the hg19 reference genome) to obtain a set of peaks. Both sets of peaks were annotated using HOMER's annotatePeaks function. Next, HAEC peaks were matched to OPC peaks through gene annotations, by taking only those peaks annotated with matching orthologous genes (only 1-to-1 orthology was considered). Matching was further restricted to promoter regions (peaks with a relative maximum distance of 2kb from the TSS). In order to ensure that peaks were true matches, this set was further restricted to a relative distance of 500 bp from each other in reference to the TSS. Using this approach a total of 7,739 peaks were matched between the HAEC and OPC datasets, including 100 peaks identified as differential in the HAEC dataset. Next, the number of reads mapped to matched peaks were obtained by counting the number of reads at the summit ± 50bp using the featureCount

package of the Subread software (v1.6.0) and the counts were normalized against the total number of reads present in all matched peaks and converted into reads per million. The significances of the read number distribution differences between the two datasets were tested using the one-sample Wilcoxon rank test with continuity correction.

Microarrays of mouse O4+ OPC gene expression and data preprocessing

Microarray analysis was performed on 6 control and 6 IL1B samples (O4+ cells isolated at P5 after *in vivo* PBS or IL1B treatment) using Agilent Whole Mouse Genome Oligo Microarrays 8x60K (Agilent). Raw data are available in Dataset S2. All the steps, from RNA extraction to statistical analysis, were performed by Miltenyi Biotec, as previously mentioned (28). In brief, Intensity data were subjected to quantile normalization, unpaired t-tests (equal variance) were conducted to compare intensities between the two groups for each probe and p values were adjusted through FDR determination by the Benjamini-Hochberg method. Fold changes correspond to the median ratios (median[IL1B]/median[PBS]). When FC<1, the FC was expressed as a negative value using the formula FC(neg)=-1/FC. For example, if FC=0.5, the indicated FC is -2. Probes with FDR <0.05 were considered significant. An additional fold change (FC) threshold was **chosen** at +/- 1.5 (corresponding to FC>1.5 and <0.666).

Heatmap representation

Heatmaps were realized with Morpheus (https://software.broadinstitute.org/morpheus). The Log2 median-centered data were visualized using a fixed (nonrelative) color pattern. The color scales are indicated on each heatmap. Rows and columns were submitted to hierarchical clustering with the following criteria: metric = one minus pearson correlation, linkage method = average.

GO term enrichment analysis

GO term Biological Pathway enrichment was done using David 6.8 (34,35).

TFBS Motif enrichment analysis, and TF footprint analysis

The 213,245 significant peaks detected by MACS2 in at least one condition (PBS or IL1B) were annotated with *HOMER annotatePeaks*. The list was restricted to the peaks located between -8000 and +8000 bp from the closest TSS ("TSS-All" list). Among this list, peaks were selected, which were annotated with a gene name, whose expression was modulated in the microarray analysis (FDR<0.05 and FC>1.5 or <-1.5,). The full list of peaks and lists restricted to up or down-regulated genes were submitted to motif enrichment analysis using *HOMER FindMotifsGenome* with the options "-size given" and "-mask". The "TSS-All" list was used as background. Six motifs corresponding to the TOP 5 motifs enriched in the full list of peaks (ISRE, IRF1, IRF2, Nfkb-p65 and PGR, figure S5B) and the 15th motif enriched in the list restricted to up-regulated genes (PU1:IRF8, figure S5B) were localized in the full list of peaks (UP+DOWN) with *HOMER FindMotifs*. For each of these motifs, the average profile of Tn5 activity was visualized using *pyDNAse* dnase_average_profile.py (11). This profiling was performed using a pooled bam file of PBS samples, or a pooled bam file of IL1B samples separately, and a pooled bam file of the two conditions ("both") together.

Testing for enrichment of paired motifs

2319 ATAC-Seq peaks corresponding to 1266 upregulated genes (886 different gene names) and 946 ATAC-seq peaks corresponding to 454 downregulated (336 different gene names) were tested for significantly enriched pairs of TFBS relative to a universe containing all the peaks located +/- 8 kb around the closest TSS. For each individual motif from the homer database, all peaks in the universe were ranked by motif occupancy using a binomial score. Then for every possible pair of motifs, peaks containing both motifs were identified using the overlap between top 5000 ranked peaks for each of the individual motifs. A hypergeometric test was used to calculate the enrichment score (p-value) for

the overlap between each test set and the peaks containing both motifs. The resulting p-values were corrected using the Benjamini-Hochberg correction.

RT-qPCR analysis and Luminex assay

Preparation of samples for quantitative reverse-transcriptase polymerase-chain reaction (qRT-PCR), primer design PCR protocol and luminex assay were similar to that previously described (36). Primer sequences are given in Table S11. *Gapdh* (glyceraldehyde-3-phosphate dehydrogenase gene) and *Rpl13* (Ribosomal Protein L13) were chosen to standardize the quantitative experiments based on reference gene suitability testing.

Statistical analysis

All *in vivo* and *in vitro* experiments were performed using an alternating treatment allocation. All analyses were performed by an experimenter blinded to the treatment groups.

The results of qRT-PCR and Luminex analyses are expressed as mean +/- SEM of at least four independent experiments. The number of analyzed samples is indicated in the legend of figures. Statistical analysis was done using the nonparametric Mann-Whitney t-test with Graphpad 5.0 software (San Diego, CA, USA). Significance is shown on the graphs (*, $p < 0.05$; **, $p < 0.01$; ***, $p < 0.001$). Specific statistical analyses for ATAC-seq and Microarray analyses are detailed in the dedicated sections of Material and Methods. The significance of intersection between the two datasets was evaluated by hypergeometric test (Phyper function) in R studio.

LIST AND LEGENDS TABLES

TABLES:

Table S1: Alignment statistics of ATAC-seq

The alignment statistics of the samples is in line with what are expected from ATAC-seq samples. Losing in the region of 10% of reads to mitochondrial alignment is usual for this type of data.

Table S2: Coordinates of the 213,246 peaks (mm10) detected in PBS and/or IL1B samples

MACS2 peak calling was run separately on PBS and IL1B pooled samples (n=3/group). The two resulting peak files (almost 200,000 peaks in each condition) were merged and the mm10 blacklist removed, leading to a list of 213,245 peaks detected in at least one condition (mm10 coordinates).

Table S3: List and annotation of the 524 differentially accessible peaks

Reads were counted in each of the 213,245 peaks (Table S2) for each sample individually (3 PBS and 3 IL1B samples). Comparison and statistical analysis with EdgeR (exact test and FDR by Benjamini-Hochberg method) identified 524 peaks with differential accessibility (FDR<0.05). Peaks were annotated using HOMER annotatePeaks.

Table S4: GO-term Biological Pathway analysis of the 524 differentially accessible peaks

GO term Biological Pathway enrichment analysis was performed on the list of gene names (478) associated with the 524 peaks (Table S3) using David6.8.

Table S5: List of the differentially expressed probes from the microarray analysis

Agilent microarray data from 6 PBS and 6 IL1B samples (O4+, P5) were submitted to t-test and FDR by Benjamini-Hochberg method. Probes with FDR<0.05 and FC>1.5 (or <-1.5) are listed in the table (Sheet 1). Up-regulated (Sheet 2) and down-regulated (sheet 3) probes are also presented separately. Red flags (columns F and G) indicate the number of undetectable samples (0 means that all samples were detected). Red and green fold change values (column K) correspond to FC>2.0 and FC<-2.0, respectively. Individual values (N to Y columns) are normalized median-centered Log2 intensities.

Table S6: GO-term Biological Pathway analysis of the UP and DOWN-regulated genes

GO-term Biological Pathway enrichment analysis was performed using David6.8 on significantly up-regulated (Sheet 1) and down-regulated genes (Sheet 2) from the microarray analysis (Table S5).

Table S7: Genes whose alterations in expression correlate to opening or closing of the chromatin

Table S8: Genes whose alterations in expression correlate to opening or closing of the chromatin in region located +/- 8kb around the TSS.

Table S9: ATAC-Seq peaks associated with upregulated genes and revealing the existence of paired TFBS motifs (see with Sascha)

Table S10: Hogan (HAECS) (list of human gene names and the corresponding orthologue genes in mice, that have been used for the Hogan Analysis

Table S11: List of the RT-qPCR primers

ACKNOWLEDGEMENTS
This work benefited from equipment and services from the iGenSeq core facility, at the Institut du Cerveau et de la Moëlle (Paris, France). We are particularly grateful to Yannick Marie, the Head of iGenSeq core facility) and Emeline Mundwiller. We are grateful to Dr Sheila Harroch (Pasteur Institute, Paris, France) for the kind gift of the Oli-neu cell line.

Figure 1

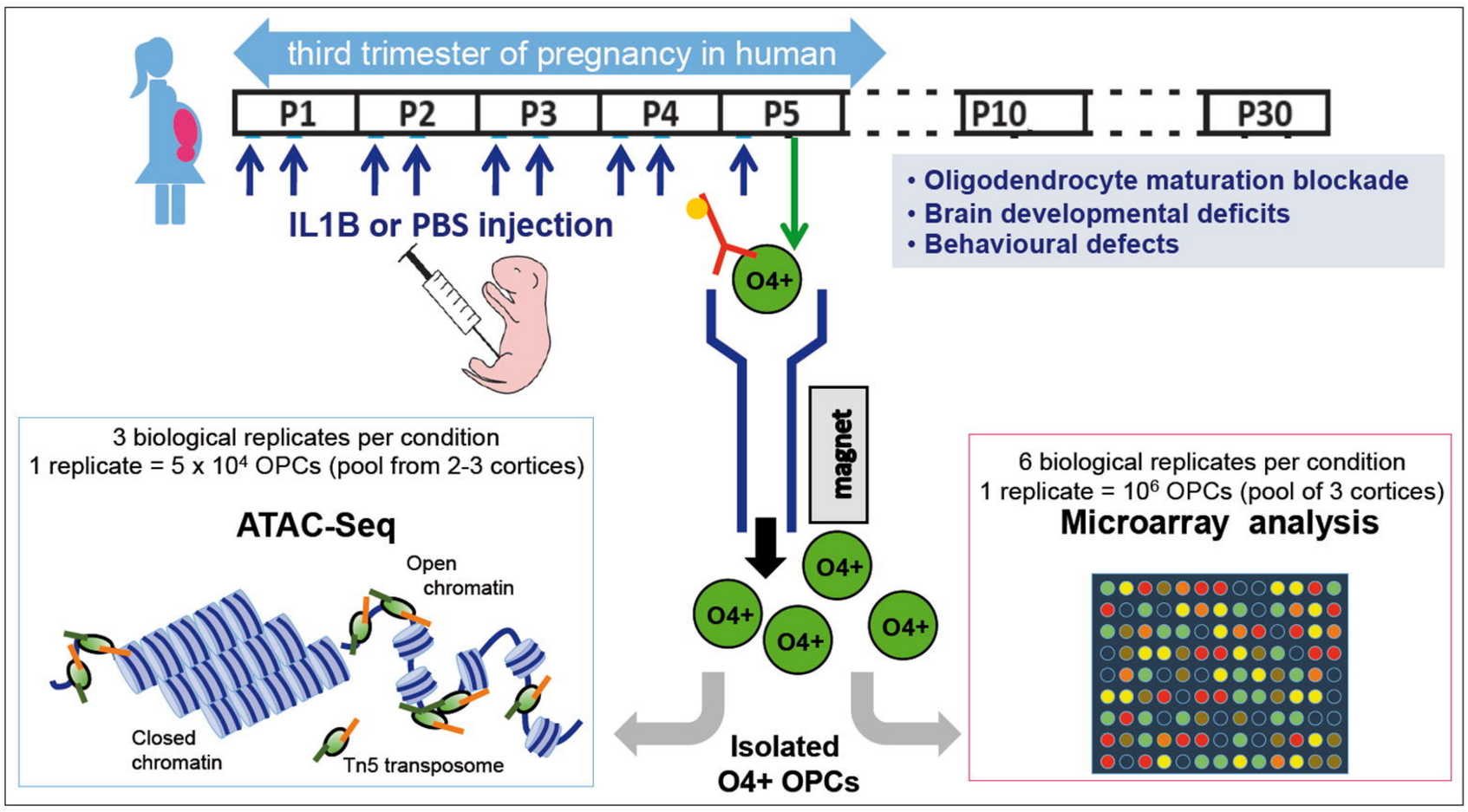
third trimester of pregnancy in human
P1
P2
P3
P4
P5
P10
P30
IL1B or PBS injection
• Oligodendrocyte maturation blockade
• Brain developmental deficits
• Behavioural defects
O4+
magnet
3 biological replicates per condition
1 replicate = 5 x 10⁴ OPCs (pool from 2-3 cortices)
ATAC-Seq
Open chromatin
Closed chromatin
Tn5 transposome
Isolated O4+ OPCs
6 biological replicates per condition
1 replicate = 10⁶ OPCs (pool of 3 cortices)
Microarray analysis

Figure 2

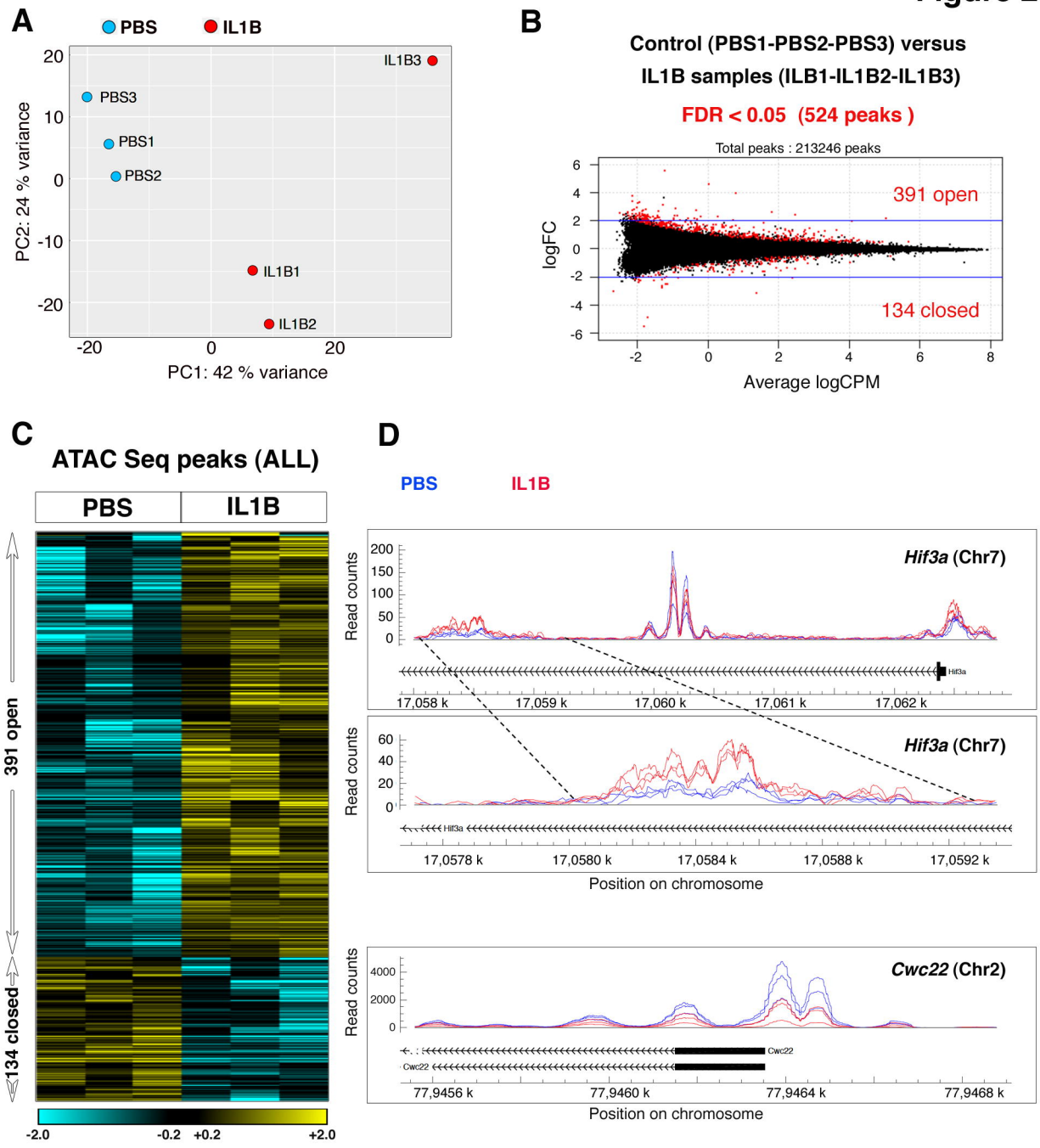
A
PBS
IL1B
IL1B3
PBS3
PBS1
PBS2
IL1B1
IL1B2
PC2: 24 % variance
PC1: 42 % variance
B
Control (PBS1-PBS2-PBS3) versus
IL1B samples (ILB1-IL1B2-IL1B3)
FDR < 0.05 (524 peaks)
Total peaks : 213246 peaks
391 open
134 closed
logFC
Average logCPM
C
ATAC Seq peaks (ALL)
PBS
IL1B
391 open
134 closed
-2.0
-0.2
+0.2
+2.0
D
PBS
IL1B
Hif3a (Chr7)
Read counts
17,058 k
17,059 k
17,060 k
17,061 k
17,062 k
17,0578 k
17,0580 k
17,0584 k
17,0588 k
17,0592 k
Position on chromosome
Cwc22 (Chr2)
77,9456 k
77,9460 k
77,9464 k
77,9468 k

Figure 3

A

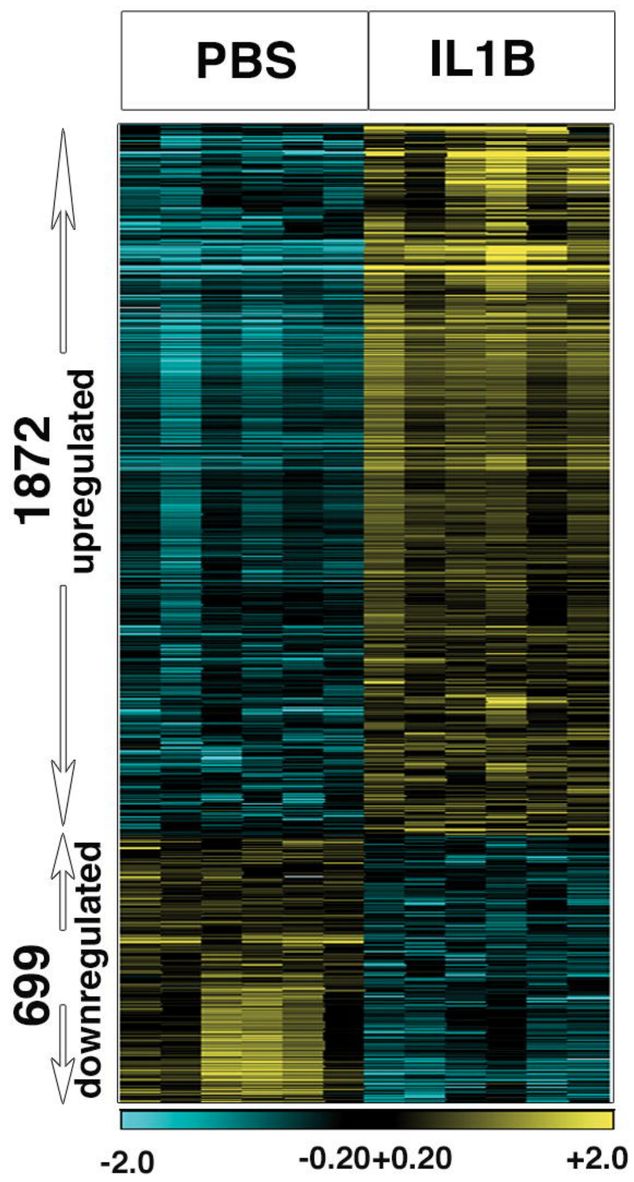

B

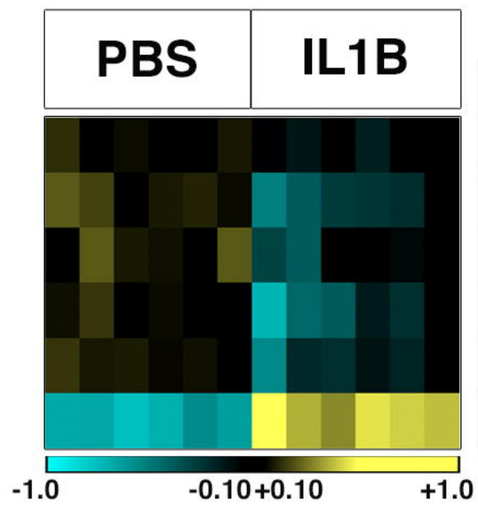

Gene	ReporterID	FC	FDR	
Mbp	A_52_P604195	-1,14	**2,51E-02**	Markers
Mbp	A_52_P329451	-1,42	**2,15E-03**	Myelination
Mog	A_66_P123582	-1,21	**1,07E-02**	Myelination
Mag	A_55_P2062757	-1,38	**1,27E-02**	Myelination
Plp1	A_55_P2069850	-1,33	**3,64E-03**	Myelination
Id2	A_52_P240542	**2,82**	**4,48E-06**	Progenitors

C

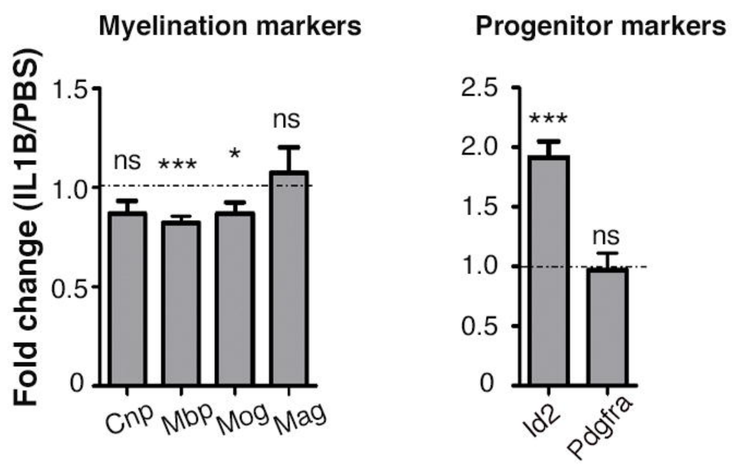

D

Category	Term	Count	PValue	Fold Enrichment	FDR
GOTERM_BP_	GO:0002376~immune system process	128	9.06E-69	6.47E+00	1.67E-65
GOTERM_BP_	GO:0006954~inflammatory response	105	8.35E-52	5.91E+00	1.54E-48
GOTERM_BP_	GO:0045087~innate immune response	102	1.89E-42	4.94E+00	3.48E-39
GOTERM_BP_	GO:0006955~immune response	69	1.64E-28	4.91E+00	3.03E-25
GOTERM_BP_	GO:0006935~chemotaxis	38	1.10E-19	6.23E+00	2.03E-16
GOTERM_BP_	GO:0051607~defense response to virus	42	2.20E-17	4.87E+00	4.06E-14
GOTERM_BP_	GO:0035458~cellular response to interferon-beta	21	1.44E-15	9.92E+00	2.66E-12
GOTERM_BP_	GO:0032496~response to lipopolysaccharide	42	1.25E-14	4.13E+00	2.31E-11
GOTERM_BP_	GO:0071222~cellular response to lipopolysaccharide	43	2.14E-14	3.98E+00	3.93E-11
GOTERM_BP_	GO:0050830~defense response to Gram-positive bacterium	28	9.00E-14	5.83E+00	1.66E-10

E

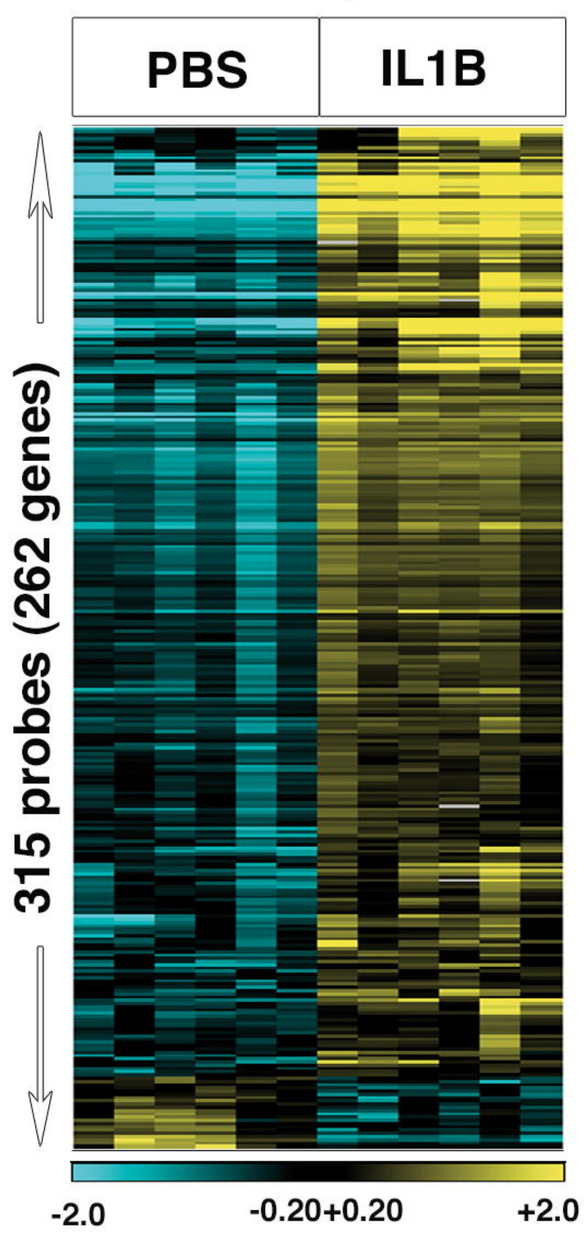

F

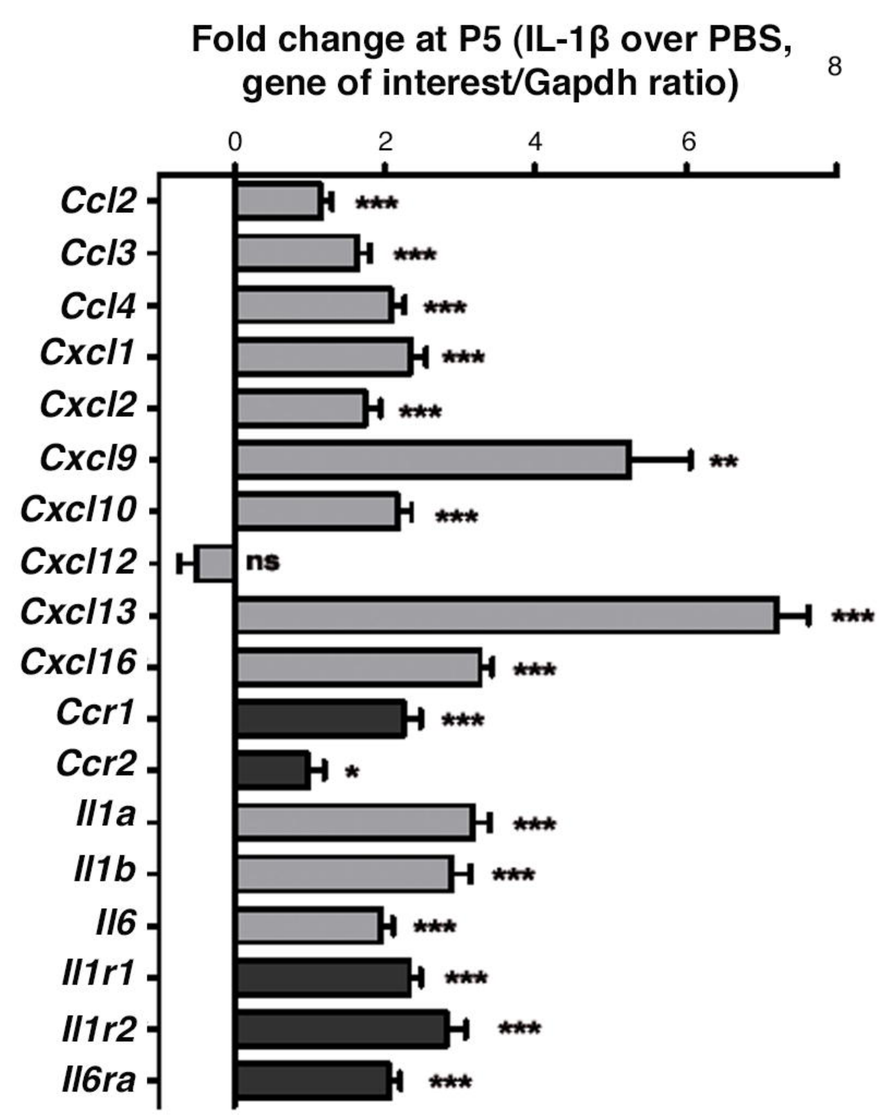

Figure 4

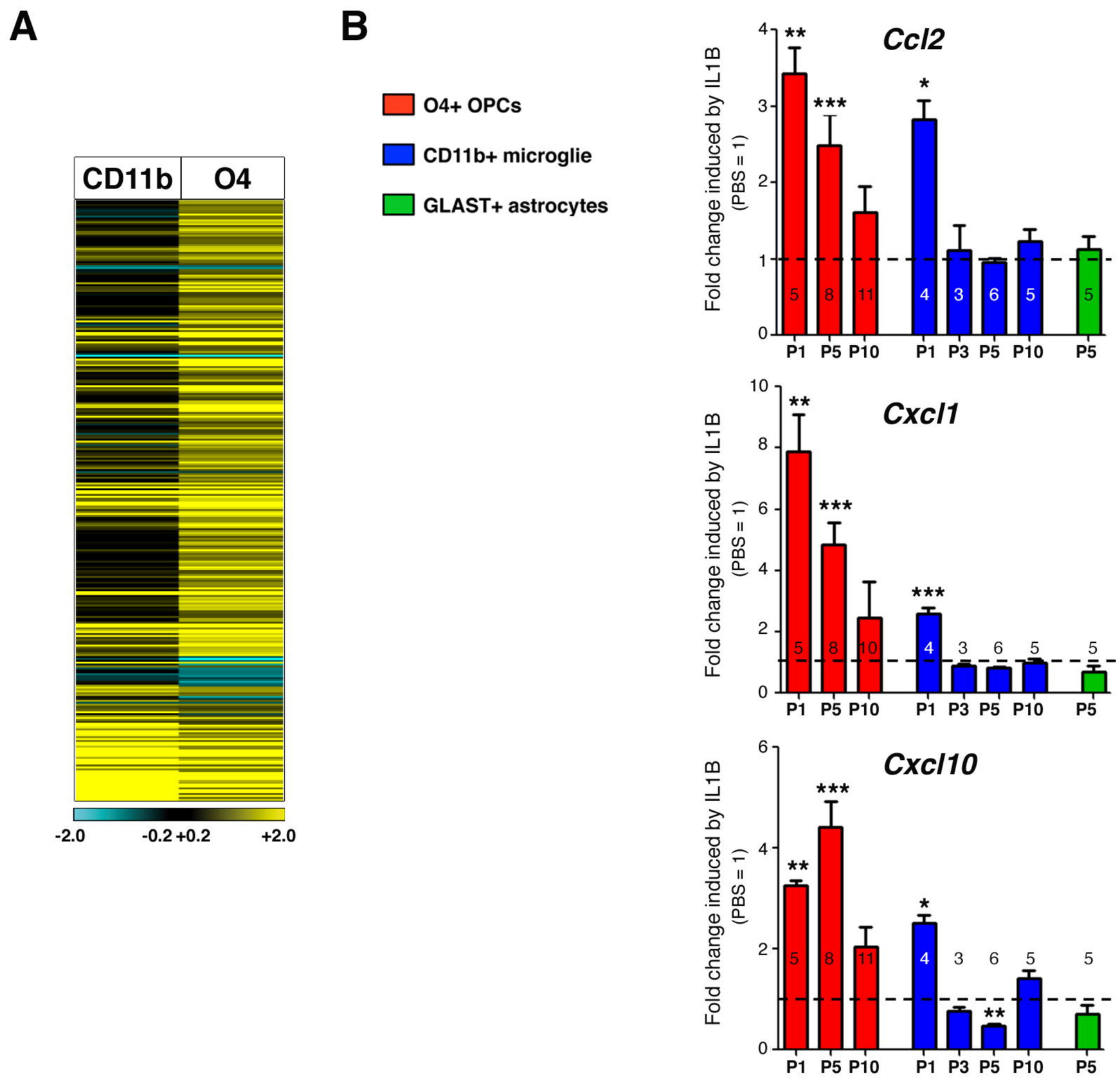
A
CD11b
O4
-2.0
-0.2 +0.2
+2.0
B
O4+ OPCs
CD11b+ microglie
GLAST+ astrocytes
Ccl2
Cxcl1
Cxcl10
Fold change induced by IL1B (PBS = 1)
P1 P5 P10 P1 P3 P5 P10 P5

Figure 5

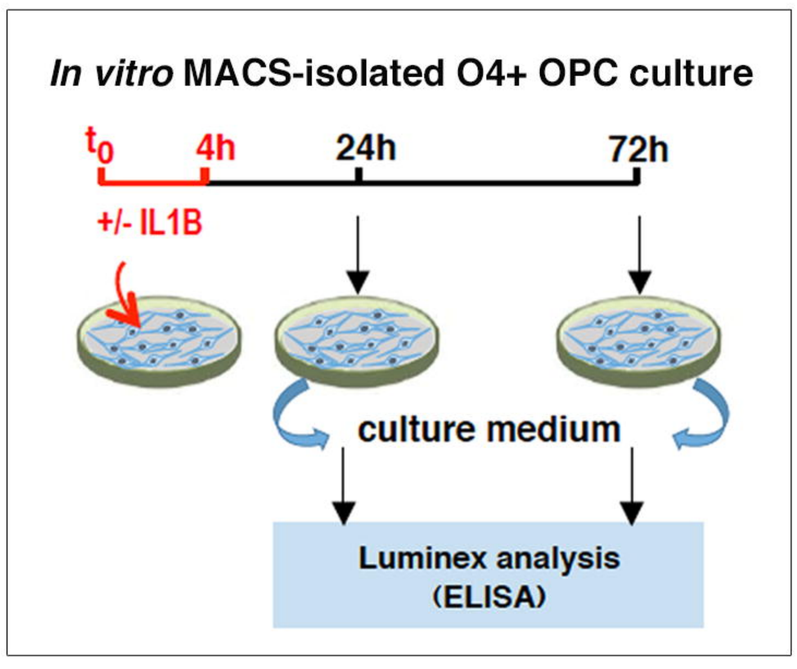
A
In vitro MACS-isolated O4+ OPC culture
t0
4h
24h
72h
+/- IL1B
culture medium
Luminex analysis
(ELISA)

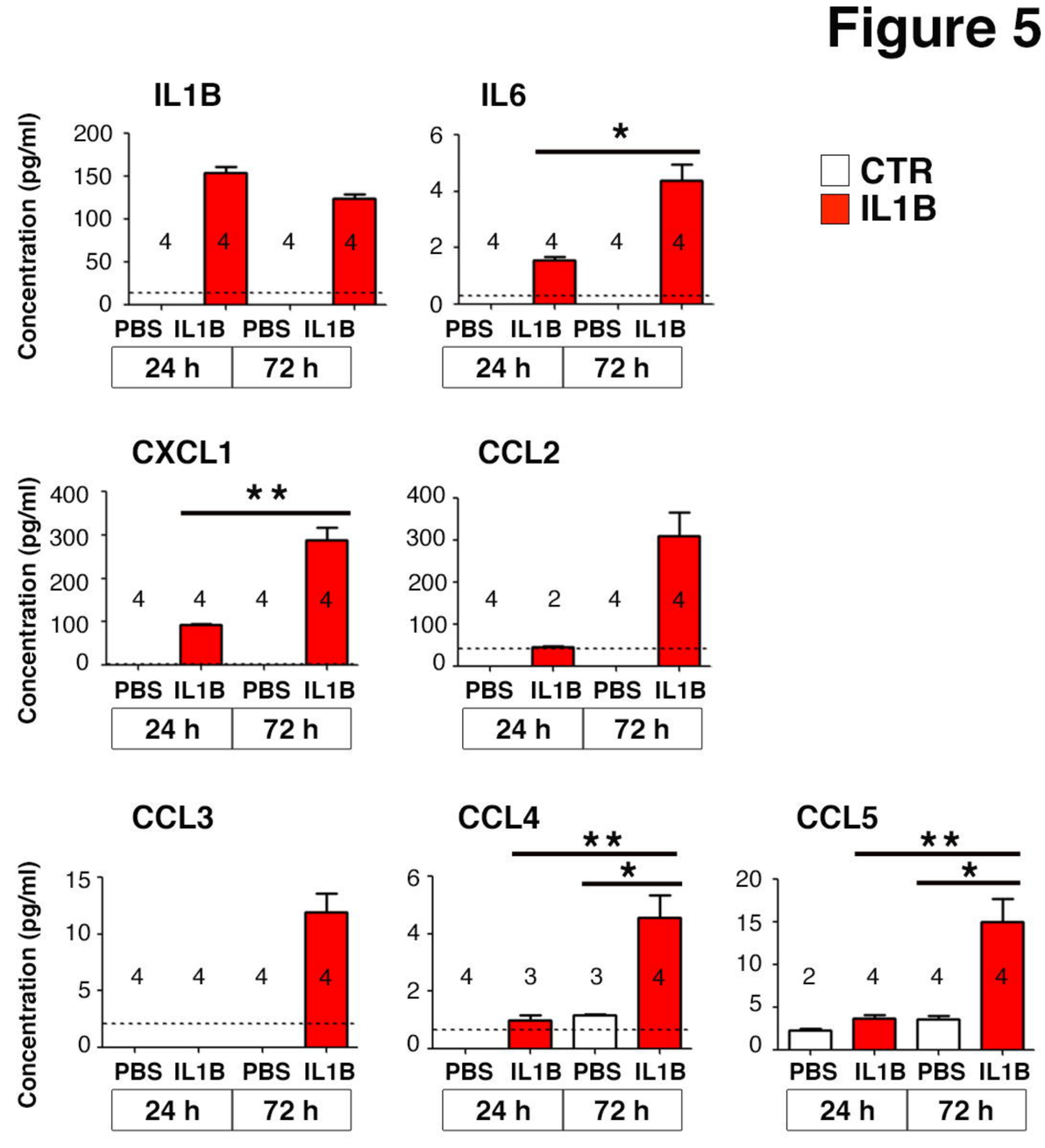
B
CTR
IL1B
IL1B
IL6
CXCL1
CCL2
CCL3
CCL4
CCL5
Concentration (pg/ml)
PBS IL1B PBS IL1B
24 h
72 h
*
**

Figure 6

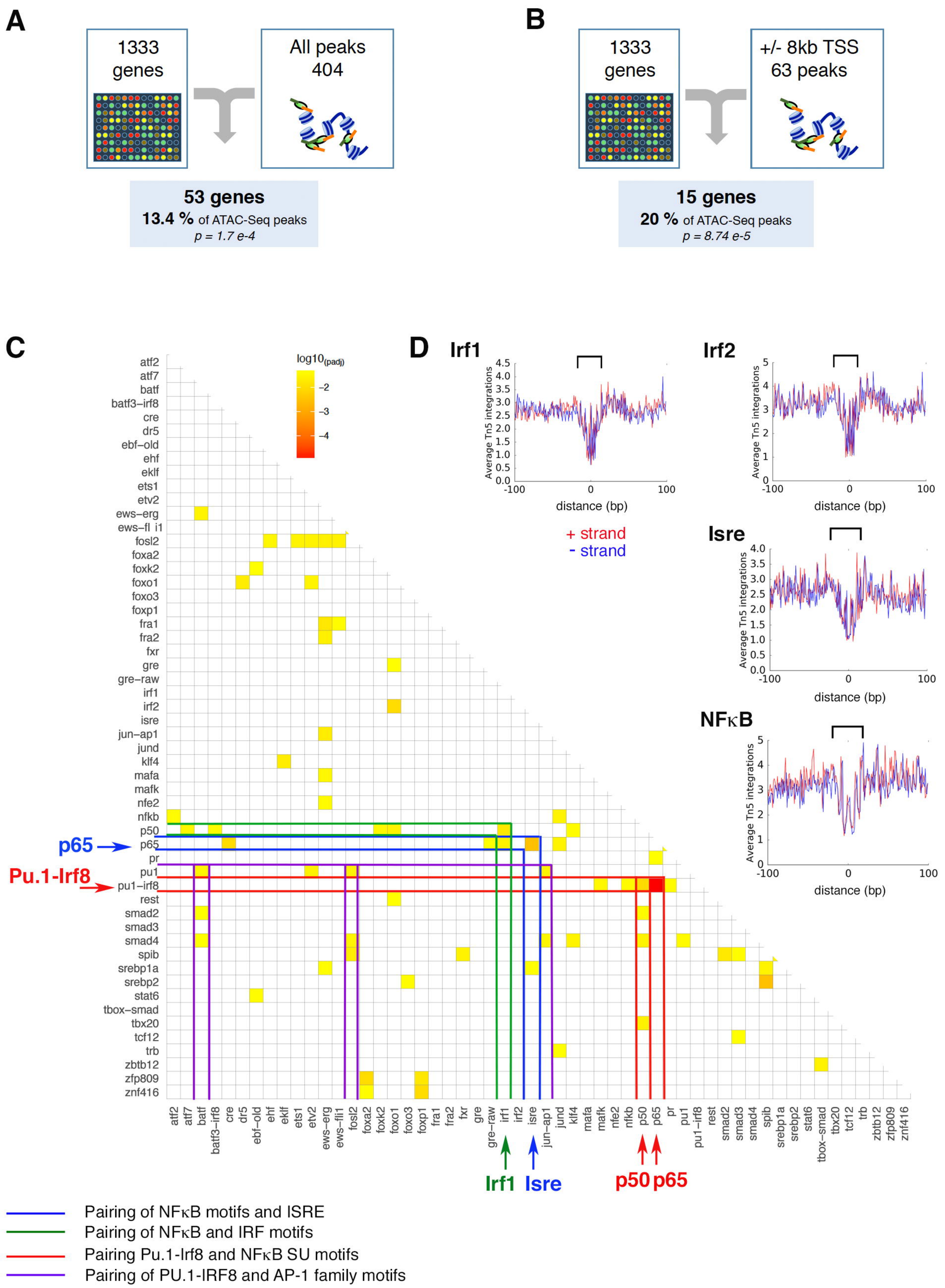
A
1333 genes
All peaks 404
53 genes
13.4 % of ATAC-Seq peaks
p = 1.7 e-4
B
1333 genes
+/- 8kb TSS 63 peaks
15 genes
20 % of ATAC-Seq peaks
p = 8.74 e-5
C
log10(padj)
−2
−3
−4
p65
Pu.1-Irf8
D
Irf1
Irf2
Isre
NFκB
Average Tn5 integrations
distance (bp)
+ strand
- strand
Irf1
Isre
p50
p65
Pairing of NFκB motifs and ISRE
Pairing of NFκB and IRF motifs
Pairing Pu.1-Irf8 and NFκB SU motifs
Pairing of PU.1-IRF8 and AP-1 family motifs

Figure 7

A

Inflammatory pathway

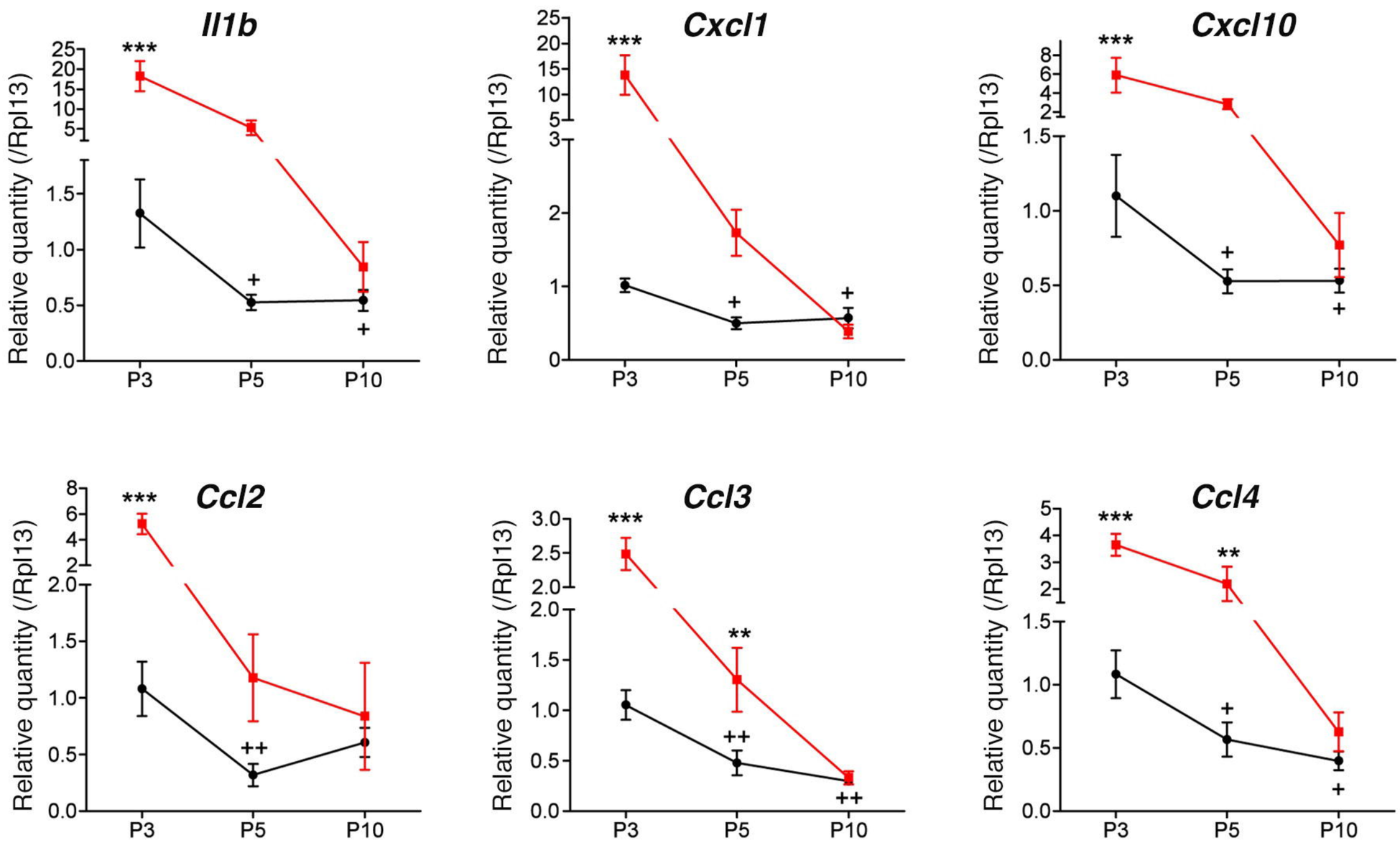

B

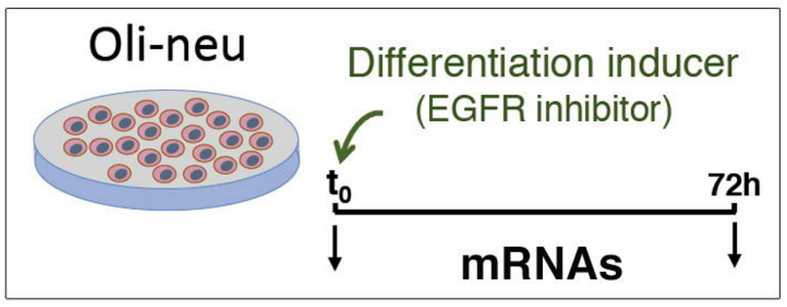

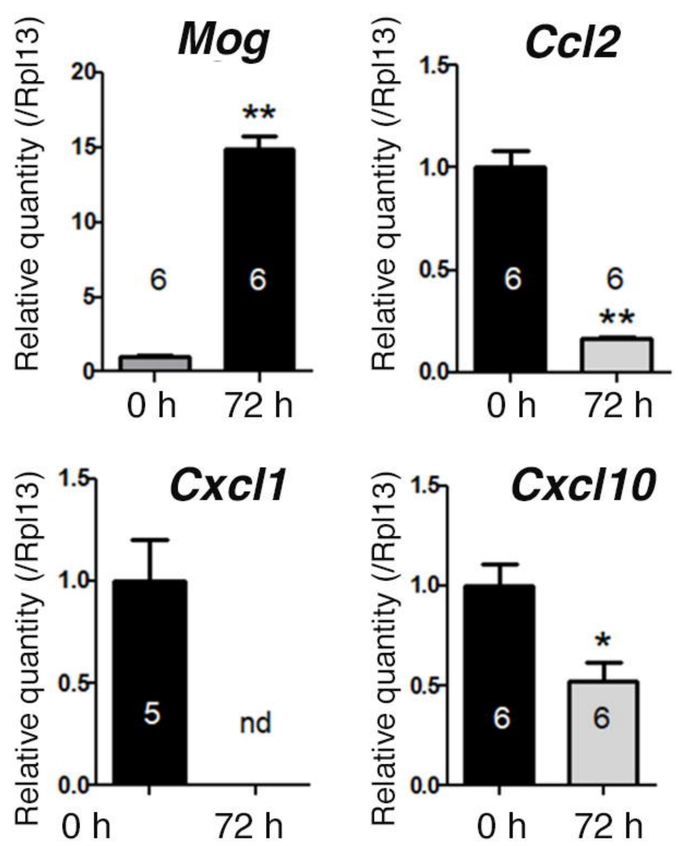
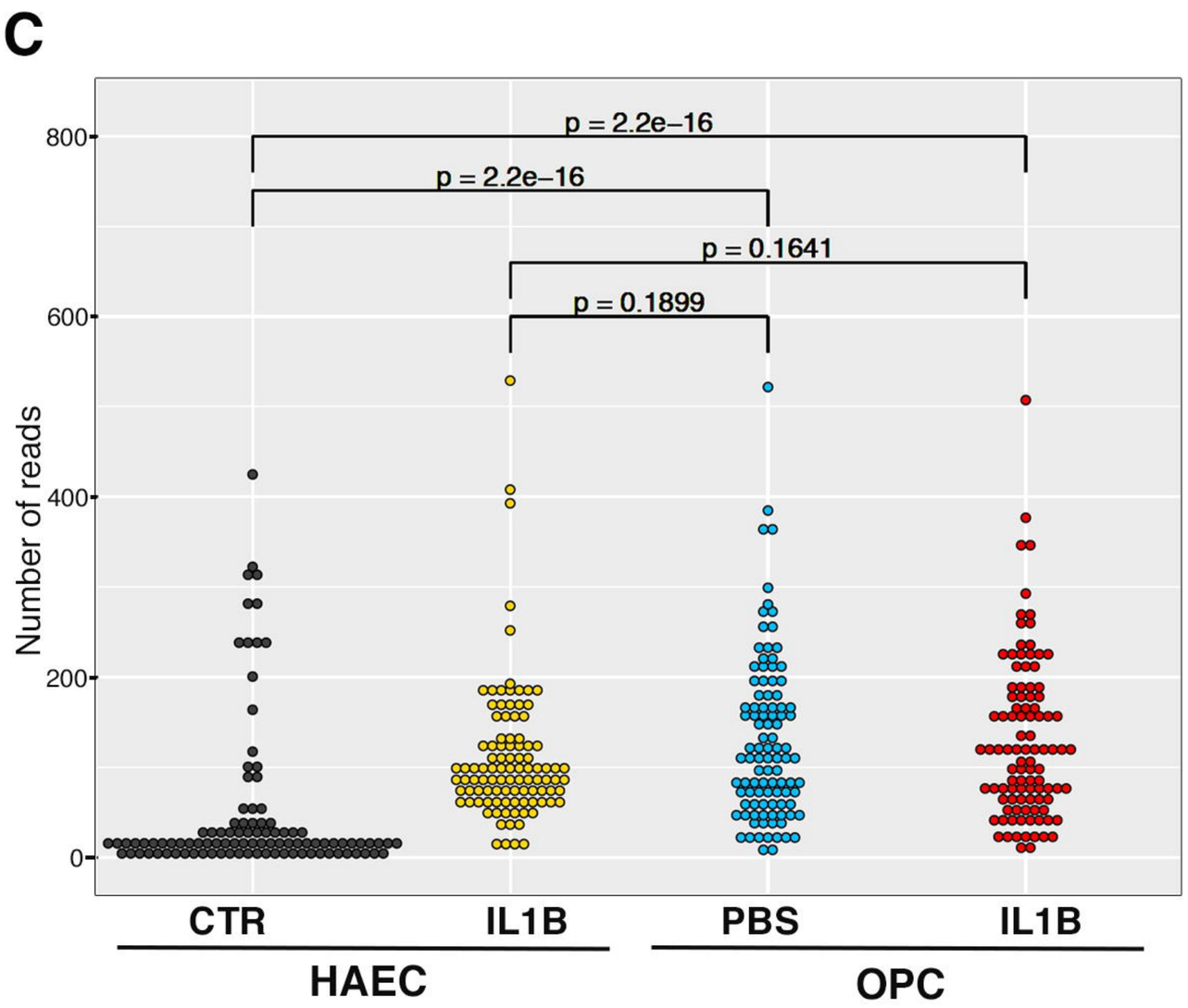
C